Supplementary Information (SI) for Journal of Materials Chemistry A.
This journal is © The Royal Society of Chemistry 2026

Supporting Information

for

Rational core-shell design of novel Ni-Co bimetallic MOF@PBA and $Al_xV_2O_5$@C as positive and negative electrode materials for high-performance aqueous Zn-ion hybrid supercapacitors

Nandini Barman[a†], Prakash Kumar Mondal[b†], Pulak Pradhan[b], Deyashi Sarkar[a], Shreya Dan[a], Nirjhar Chakraborty[a], Pallav Mondal[b], Dudekula Khasim Vali[b], Joydeep Ray[c], Yogesh Kumar[d], Utpal Adhikari[b], Milan Maji[b], Subhradeep Mistry[e], Sourav Laha[b*] and Anjan Banerjee[a*]

[a] Department of Chemistry, Presidency University, Kolkata, 86/1 College Street, Kolkata-700073, India

[b] Department of Chemistry, National Institute of Technology Durgapur, Durgapur-713209, India

[c] Department of Chemistry, Indian Institute of Technology Patna, Bihar-801106, India

[d] Department of Chemistry, Miranda House, University of Delhi, Delhi-110007, India

[e] Department of Chemistry, Hemvati Nandan Bahuguna Garhwal University, Tehri, Uttarakhand-249199, India

*slaha.ch@nitdgp.ac.in & anjan.chem@presiuniv.ac.in

[†] These authors contributed equally to this work as co-first authors.

Contents	**Page No.**
Section S1: Synthesis of Prussian Blue Analogues (PBAs)	S3
Section S2: Methodology for calculating diffusion coefficient (D) from EIS data	S4
Table S1: Literature survey and comparative analysis of capacitive performances for Zn-ion hybrid supercapacitors	S4-S6
Table S2: Crystal Data and Structure Refinement Parameters	S7
Table S3: Bond length (M-O) data of NCBMOF-11	S8
Table S4: Bond angle (M-O-M) data of NCBMOF-11	S8
Table S5: Crystal lattice parameters and CCDC numbers for the reported MOFs with BTC linker	S8-S11
Table S6: ICP-OES results of NCBMOF-11, NCBMOF-12, and NCBMOF-21	S11
Table S7: Rietveld refinement parameters of NCBMOF@PBA-21 and AlVO	S11-S12
Table S8: R_S and R_{CT} data for NCBMOF-12 and NCBMOF@PBA-12 positive electrodes at before and after cycling test	S12
Table S9: R_S and R_{CT} data for AlVO and AlVO@C negative electrodes at before and after cycling test	S12
Table S10: R_S and R_{CT} data for NCBMOF@PBA-12//AlVO@C full cells at before and after cycling test	S12
Figure S1. Asymmetric unit of NCBMOF-11	S13
Figure S2: (a) 2D layer and (b) view of 2D layers along the crystallographic a-axis of NCBMOF-11	S14
Figure S3: PXRD refinement plot of (a) NCBMOF-11 and (b) NCBMOF-21	S15
Figure S4: (a) CHNS and (b) oxygen analysis data of NCBMOF-11	S16
Figure S5: PXRD plots of AlVO and AlVO@C	S17
Figure S6: FESEM-EDX data of NCBMOF-11	S18
Figure S7: FESEM-EDX data of NCBMOF-12	S19
Figure S8: HAADF-STEM EDX data of NCBMOF-12	S20
Figure S9: FESEM-EDX data of NCBMOF-21	S21
Figure S10: FESEM-EDX data of NCBMOF@PBA-12	S22
Figure S11: HAADF-STEM EDX data of NCBMOF@PBA-12	S23
Figure S12: FESEM-EDX data of AlVO	S24
Figure S13: FESEM-EDX data of AlVO@C	S25
Figure S14: HAADF-STEM EDX data of AlVO	S26
Figure S15: HAADF-STEM EDX data of AlVO@C	S27
Figure S16: HRTEM images showing lattice fringes: (a) NCNMOF@PBA-12 and (b) ALVO@C	S28
Figure S17: Pore size distribution plots of (a) NCBMOF-12 and (b) NCBMOF@PBA-12	S28
Figure S18: Raman spectra of NCBMOF-11, NCBMOF-12 and NCBMOF-21	S29
Figure S19: C 1s deconvoluted spectra of NCBMOF-12 and NCBMOF@PBA-12	S30
Figure S20: C 1s deconvoluted spectra of AlVO@C	S30
Figure S21: CV of (a) NCBMOF-11, (b) NCBMOF-21; b-value calculation of (c) NCBMOF-11, (d) NCBMOF-21	S31
Figure S22: CV profiles of (a) PBA-11, (b) PBA-12, (c) PBA-21; b-value calculations for (d) PBA-11, (e) PBA-12, (f) PBA-21	S32
Figure S23: CV of (a) NCBMOF@PBA-11, (b) NCBMOF@PBA-21; b-value calculation of (c) NCBMOF@PBA-11, (d) NCBMOF@PBA-21	S33
Figure S24: b-value calculation of (a) NCBMOF-12, (b) NCBMOF@PBA-12, (c) AlVO, (d) AlVO@C	S34

Figure S25: GCD of (a) NCBMOF-11, (b) NCBMOF-21, (c) comparison of rate capability among three compositions namely NCBMOF-11, NCBMOF-12 and NCBMOF-21	S365
Figure S26: GCD of (a) PBA-11, (b) PBA-12, (c) PBA-21, (d) comparison of rate capability among three compositions	S36
Figure S27: GCD of (a) NCBMOF@PBA-11, (b) NCBMOF@PBA-21, (c) comparison of rate capability among three compositions namely NCBMOF@PBA-11, NCBMOF@PBA-12 and NCBMOF@PBA-21	S37
Figure S28: ex situ XPS analysis of NCBMOF@PBA-12 at its charged and discharged states: (a) Ni 2p, (b) Co 2p, and (c) Fe 2p spectra	S38
Figure S29: Nyquist plots at before and after cycling: (a) NCBMOF-12 and (b) NCBMOF@PBA-12	S39
Figure S30: ex situ XPS analysis of AlVO at charged and discharged states	S39
Figure S31: Nyquist plots at before and after cycling: (a) AlVO and (b) AlVO@C	S40
Figure S32: SEM images comparing the surface morphologies of AlVO and AlVO@C negative electrodes in their initial pristine state and after prolonged electrochemical cycling (50,000 CV at a scan rate of 25 mV s^{-1})	S40-S41
Figure S33: GCD profiles of the NCBMOF@PBA-12//AlVO@C full cells under (a) 0-1.2 V and (b) 0-1.8 V window	S41
Figure S34: Nyquist plots at before and after full cell cycling at variable voltage regime: (a) 0-1.2 V, (b) 0-1.5 V and (c) 0-1.8 V	S41
Figure S35: Surface morphology of NCBMOF@PBA-12 positive and AlVO@C negative electrodes at before and after cycling test @ 1 A g-1	S42
Figure S36: Comparative PXRD patterns of pristine active material and corresponding cycled electrodes (@ 1 A g-1)	S43
References	S44

Section S1. Synthesis of Prussian Blue Analogues (PBAs): Three NiCo-PBAs with different Ni/Co ratios were synthesized using the same citrate-assisted crystallization route.[S1] For $K_2Ni_{0.5}Co_{0.5}Fe(CN)_6$ (PBA-11), 2.5 mmol $CoCl_2$, 2.5 mmol $NiCl_2$, and 5 mmol trisodium citrate were dissolved in 50 mL of DI water. In a separate beaker, 5 mmol $K_4[Fe(CN)_6$ was dissolved in 50 mL deionized (DI) water. The two solutions were then simultaneously added dropwise into 100 mL DI water and stirred for 2 h at room temperature. The resulting olive-green precipitate was collected by centrifugation (5000 rpm, 30 min), thoroughly washed with DI water and ethanol, and dried at 70 °C for 8 h. However, the PBA-12 (Ni:Co = 1:2) and PBA-21 (Ni:Co = 2:1) were prepared following the same procedure by adjusting the Ni and Co precursor ratios accordingly.

Section S2. Methodology for calculating diffusion coefficient (D) from EIS data: The lower-frequency Warburg component of the Nyquist plot is used to estimate the diffusion coefficient (D) of Zn^{2+} ions within the bulk of electrode. The formula for determining D is provided in **Eq. S1**.[S2]

$D = 0.5 \times R^2 \times T^2 \times A^{-2} \times n^{-4} \times F^{-4} \times C^{-2} \times \sigma^{-2}$ ………………………………………………….……… **(Eq. S1)**

where R is the universal gas constant, T is the absolute temperature, A is the electrode's geometric area, n is the number of electrons transferred per molecule during oxidation and reduction, F is the Faraday constant, C is the molar concentration of Zn^{2+} ions (mol cm^{-3}), and σ is the Warburg factor, which relates to the real component of impedance (Z') via the following **Eq. S2**:

$Z' = R_s + R_{CT} + \sigma\omega^{-1/2}$ ……………………………………………………………..........….. **(Eq. S2)**

where ω represents the frequency in the EIS measurement. The linear dependence of Z′ on $\omega^{-1/2}$ indicates Warburg-type diffusion behaviour. From this plot, the slope represents the Warburg factor (σ), whereas the intercept corresponds to the combined resistance of the solution R_S and R_{CT}.

Supporting Tables

Table S1: Literature survey and comparative analysis of capacitive performances for Zn-ion hybrid supercapacitors.

Sr	**Positive Electrode**	**Negative Electrode**	**Electrolyte**	**Performances**	**Ref**
1	N, P, O co-doped carbon	Zn	$ZnSO_4$	215.2 F g^{-1} @ 0.1 A g^{-1} within 0.2-1.8 V; 54.4 Wh kg^{-1} @ 4000 W kg^{-1}; ~100% capacitance retention over 10,000 cycles @ 5 A g^{-1}.	S3
2	MOF derived porous carbon (MPC)	Zn	$Zn(CF_3SO_3)_2$	289.2 F g^{-1} @ 0.2 A g^{-1} within 0-1.8 V; 130.1 Wh kg^{-1} @ 180.3 W kg^{-1}; 7.8 kW kg^{-1} @ 56 Wh kg^{-1}; 96.7% capacitance retention after 10,000 cycles @ 10 A g^{-1}.	S4

3	Reduced graphene oxide (rGO)	Zn	$ZnSO_4$	277 F g^{-1} & 75.4 Wh kg^{-1} @ 1 mV s^{-1} within 0.2-1.6 V; 97.8% capacitance retention over 20,000 cycles @ 2.5 A g^{-1}.	S5
4	N, S co-doped porous carbons (NSPCs)	Zn	$Zn(CF_3SO_3)_2$	273 F g^{-1} @ 0.1 A g^{-1} within 0-1.8 V; 122.6 Wh kg^{-1} @ 58.3 W kg^{-1}; 14.46 kW kg^{-1} @ 77.9 Wh kg^{-1}; 99.5% capacitance retention after 15,000 cycles @ 5 A g^{-1}.	S6
5	MnO_2-CNT	MXene ($Ti_3C_2T_x$)	$ZnSO_4$ + $MnSO_4$	115.1 F g^{-1} @ 1 mV s^{-1} within 0-0.8 V; 98.6 Wh kg^{-1} @ 77.5 W kg^{-1}; 2480.6 W kg^{-1} @ 29.7 Wh kg^{-1}; 83.6% capacitance retention after 15,000 cycles @ 5.2 A g^{-1}.	S7
6	Ti_3C_2	Zn	$ZnSO_4$	132 F g^{-1} @ 0.5 A g^{-1} within 0.1-1.35 V; 82.5% capacitance retention after 1,000 cycles @ 3 A g^{-1}.	S8
7	N-Ti_3C_2	Zn	$ZnSO_4$	247.9 F g^{-1} @ 0.1 A g^{-1} within 0.05-1.2 V; 45.54 Wh kg^{-1} @ 70 W kg^{-1}; 4093 W kg^{-1} @ 30.99 Wh kg^{-1}; 88.34% capacitance retention after 6,000 cycles @ 1.5 A g^{-1}.	S9
8	TiN	Zn	$ZnSO_4$	489.8 F g^{-1} @ 0.2 A g^{-1} within 0.1-1.9 V; 135 Wh kg^{-1} @ 186 W kg^{-1}; 3472 W kg^{-1} @ 56 Wh kg^{-1}; ~78 % capacitance retention after 10,000 cycles @ 1 A g^{-1}.	S10
9	Molten salt assisted pitch derived porous carbon (MSPC)	Zn	$ZnSO_4$	136.5 F g^{-1} @ 0.68 A g^{-1} within 0-1.8 V; 36.5 Wh kg^{-1} @ 376.6 W kg^{-1}; 3.2 kW kg^{-1} @ 22.7 Wh kg^{-1}; 85.4 % capacitance retention after 10,000 cycles @ 5.44 A g^{-1}.	S11
10	Cross-linked N & P co-incorporated	Zn	$ZnSO_4$	233 F g^{-1} @ 0.5 A g^{-1} within 0.2-1.8 V; 81.1 Wh kg^{-1} @ 80 W kg^{-1};	S12

	porous carbon nanosheets			13.36 kW kg^{-1} @ 40 Wh kg^{-1}; 101.8% capacitance retention after 10,000 cycles @ 5 A g^{-1}.	
11	Carbon cloth@ZIF-8	Zn	$ZnSO_4$	302 F g^{-1} @ 0.5 A g^{-1} within 0.2-1.8 V; 107.4 Wh kg^{-1} @ 0.4 kW kg^{-1}; 16.2 kW kg^{-1} @ 65.9 Wh kg^{-1}; ~100% capacitance retention after 10,000 cycles @ 1 A g^{-1}.	S13
12	Poly(3,4-ethylenedioxythiophene) coated $Na_{0.55}MnO_2$@ carbon cloth	Polyimide @MWCNT	$ZnSO_4$	110.7 F g^{-1} @ 5 mV s^{-1} within 0-2 V; 10.7 Wh kg^{-1} @ 192.2 W kg^{-1}; 1000 W kg^{-1} @ 6 Wh kg^{-1}; 82.1% capacitance retention after 2,000 cycles @ 15 mV s^{-1}.	S14
13	$Na_{0.11}MnO_2$/graphene	Activated Carbon	$ZnSO_4$ + $MnSO_4$	165 F g^{-1} @ 0.5 A g^{-1} within 0-1.8 V; 74.3 Wh kg^{-1} @ 455.7 W kg^{-1}; 9.6 kW kg^{-1} @ 18 Wh kg^{-1}; 83% capacitance retention after 5,000 cycles @ 1 A g^{-1}.	S15
14	rGO-V_2O_5	rGO-MXene	$ZnSO_4$	175 F g^{-1} @ 0.5 mV s^{-1} within 0-1.6 V; 107.2 Wh kg^{-1} @ 321.6 W kg^{-1}; 2780 W kg^{-1} @ 61.4 Wh kg^{-1}; 81% capacitance retention after 10,000 cycles @ 0.2 A g^{-1}.	S16
15	CNTs@MnO_2	Nb_2CT_x	$ZnSO_4$+ $MnSO_4$	192.8 F g^{-1} @ 1 mV s^{-1} within 0-1.8 V; 96.7 Wh kg^{-1} @ 183.2 W kg^{-1}; 1156.3 W kg^{-1} @ 61 Wh kg^{-1}; 88.7% capacitance retention after 10,000 cycles @ 2 A g^{-1}.	S17
16	**NCB MOF@PBA-12**	**$Al_xV_2O_5$ @C**	**$ZnSO_4$**	**450 F g^{-1} @ 1 A g^{-1} within 0-1.8 V, 203 Wh kg^{-1} @ 900 W kg^{-1}; 9000 W kg^{-1} @ 158 Wh kg^{-1}; 71% capacitance retention after 5,000 cycles @ 5 A g^{-1}.**	**This Work**

Table S2: Crystal Data and Structure Refinement Parameters.

Structural Parameter	**NCBMOF-11 (Single crystal)**	**NCBMOF-12 (Rietveld refinement)**	**NCBMOF-21 (Rietveld refinement)**
Empirical formula	$C_7H_9NO_5Ni_{0.5}Co_{0.5}$	$C_7H_9NO_5Ni_{0.33}Co_{0.67}$	$C_7H_9NO_5Ni_{0.67}Co_{0.33}$
Crystal system	Trigonal	Trigonal	Trigonal
Crystal colour	Dark pinkish green	Dark pinkish green	Light pinkish green
Crystal shape	block	block	block
Space group	*P-3* (no.147)	*P-3* (no.147)	*P-3* (no.147)
a[Å]	13.9082(5)	13.958(1)	13.898(2)
b[Å]	13.9082(5)	13.958(1)	13.898(2)
c[Å]	8.0810(3)	8.099(1)	8.031(1)
α [°]	90	90	90
β [°]	90	90	90
γ [°]	120	120	120
V[Å^3]	1353.75(11)	1366.68(25)	1343.50(25)
T[K]	293(2)	298	298
ρ [calc., g cm^{-3}]	1.811	1.792	1.823
μ[mm^{-1}]	1.896	--------	--------
λ	0.71073 [Mo Kα/Å]	1.5406 [Cu Kα/Å]	1.5406 [Cu Kα/Å]
θ range [°]	1.691-31.007	5-60	5-60
R_{int}	0.0331	--------	--------
R indexes [1>2σ (l)]	$R_1 = 0.0454$ $wR_2 = 0.1172$	--------	--------
R indexes (all data)	$R_1 = 0.0540$; $wR_2 = 0.1229$	--------	--------
R indexes (from Rietveld refinement)	--------	$WR_P = 0.0760$ $R_P = 0.0532$	$WR_P = 0.1081$ $R_P = 0.0748$
χ^2 (from Rietveld refinement)	--------	1.57	2.38

[a] $R_1 = \sum|F_o| - |F_c||/\sum|F_o|$; $wR_2 = \{\sum[w(F_o^2 - F_c^2)]/\sum[w(F_o^2)^2]\}^{1/2}$. $w = 1/[\rho^2(Fo)^2 + (aP)^2 + bP]$. $P = [\max(F_o, O) + 2(F_c)^{-2}]/3$ where a = 0.0783 and b = 0 for NCBMOF-11

Table S3: Bond length (M-O) data of NCBMOF-11.

Atom1	Atom2	Length (Å)
Co1	O1	2.027(3)
Co1	O2	2.040(2)
Co1	O3	2.123(2)
Co1	O4	2.113(2)
Co1	O5	2.086(3)

Table S4: Bond angle (M-O-M) data of NCBMOF-11.

Atom1	Atom2	Atom3	Angle (°)
O2	Co1	O4	90.01(8)
O2	Co1	O3	90.42(8)
O2	Co1	O1	86.69(9)
O2	Co1	O4	177.25(8)
O2	Co1	O5	92.99(9)
O4	Co1	O3	178.86(8)
O4	Co1	O1	96.04(9)
O4	Co1	O4	88.83(8)
O4	Co1	O5	94.78(9)
O3	Co1	O1	85.05(9)
O3	Co1	O4	90.79(9)
O3	Co1	O5	84.14(9)
O1	Co1	O4	90.95(9)
O1	Co1	O5	169.2(1)
O4	Co1	O5	89.59(9)

Table S5: Crystal lattice parameters and CCDC numbers for the reported MOFs with BTC linker.

Compound	**Crystal Lattice Parameters**	**CCDC No.**	**References**
Catena-[tetrakis(μ-benzene-1,3,5-tricarboxylato)-bis(μ-6amino-7H-purin-7-yl)-triaqua-hexa-zinc unknown solvate]	Space Group: *P-1* (2), a (Å) 14.208 b (Å) 17.229 c (Å) 26.158 α (˚) 88.764 β (˚) 74.470 γ (˚) 70.377	1057226	*Angewandte Chemie, International Edition*, 2015, **54**, 10454.
tetrakis(μ-benzene-1,3,5-tricarboxylato)-hexatricontacarbonyl-dodeca-osmium dichloromethane n-hexane solvate	Space Group: P -1 (2), a (Å) 16.096 b (Å) 17.128 c (Å) 26.844 α (˚) 88.620 β (˚) 88.628 γ (˚) 63.616	1949184	*Inorganic Chemistry Communications*, 2020, **121**, 108212.

catena-(bis(μ_6-Benzene-1,3,5-tricarboxylato)-tetrakis(N,N-dimethylformamide)-tri-magnesium(ii))	Space Group: P 2_1/c (14), a (Å) 17.490 b (Å) 11.940 c (Å) 18.460 α (˚) 90.00 β (˚) 116.870 γ (˚) 90.00	887454	*Inorganica Chimica Acta*, 2013, **394**, 452.
catena-(bis(μ_3-Benzene-1,3,5-tricarboxylato)-(μ_3-benzene-1,3,5-tricarboxyilic acid)-hexakis(N,N-dimethylformamide)-tri-magnesium(ii))	Space Group**:** P 6_3/m (176), a (Å) 16.596 b (Å) 16.596 c (Å) 14.351 α (˚) 90 β (˚) 90 γ (˚) 120.00	887452	*Inorganica Chimica Acta*, 2013, **394**, 452.
catena-(tris(trimethylammonium)tris(μ_3-benzene-1,3,5-tricarboxylato)-hexakis(N,N-dimethylformamide)-tri-magnesium(ii))	Space Group: P 6_3/m (176), a (Å) 16.596 b (Å) 16.596 c (Å) 14.351 α (˚) 90.00 β (˚) 90.00 γ (˚) 120.00	887453	*Inorganica Chimica Acta*, 2013, **394**, 452.
Ni-BTC(solvent:An1)	Space Group**:** P -3 (147), a (Å) 11.003 b (Å) 11.003 c (Å) 7.045 α (˚) 90.00 β (˚) 90.00 γ (˚) 120.00	1941312	*Quimica Nova*, 2016, **39**, 669.
Ni-BTC(solvent:DMF)	Space Group: P 2_1/c (14), a (Å) 12.772 b (Å) 21.245 c (Å) 24.620 α (˚) 90.00 β (˚) 111.021 γ (˚) 90.00	1941313	*Quimica Nova*, 2016, **39**, 669.
Ni-BTC(solvent:EtOH)	Space Group: P 2_1/c (14), a (Å) 8.340 b (Å) 31.240 c (Å) 24.620 α (˚) 90.00 β (˚) 117.833 γ (˚) 90.00	1941314	*Quimica Nova*, 2016, **39**, 669.

Ni-BTC(solvent: NaOH/NH_4OH)	Space Group: C 2/c (15), a (Å) 24.628 b (Å) 6.552 c (Å) 13.291 α (˚) 90.00 β (˚) 116.011 γ (˚) 90.00	1941315	*Quimica Nova*, 2016, **39**, 669.
Ni-BTC(solvent:Pyr)	Space Group: P 2_1/c (14), a (Å) 12.772 b (Å) 21.245 c (Å) 24.620 α (˚) 90.00 β (˚) 111.021 γ (˚) 90.00	1941316	*Quimica Nova*, 2016, **39**, 669.
Ni-BTC(solvent:TMA)	Space Group: P -1 (2), a (Å) 8.804 b (Å) 8.842 c (Å) 15.885 α (˚) 77.424 β (˚) 88.961 γ (˚) 61.332	1941317	*Quimica Nova*, 2016, **39**, 669.
$C_{72} H_{12} O_{60} Os_{12}$	Space Group: P -1 (2), a (Å) 16.096 b (Å) 17.128 c (Å) 26.844 α (˚) 88.620 β (˚) 88.628 γ (˚) 63.616	2185269	*Inorganic Chemistry Communications*, 2020, **121**, 108212.
$(C_9H_3O_{24}Tb)_n$,$2H_2O$	Space Group**:** P 4_3 2 2 (95), a (Å) 10.279 b (Å) 10.279 c (Å) 14.538 α (˚) 90.00 β (˚) 90.00 γ (˚) 90.00	2227727	*Journal of the American Chemical Society*, 2005, **127**, 1504.
4$(C_{18}H_{12}Cu_3O_{15})$n, $GeO_{44}W_{12}^{2-}$, $C_4H_{24}N^+$,12(H_2O)	Space Group: F m -3 m (225), a (Å) 26.318 b (Å) 26.318 c (Å) 26.318	2227728	*Journal of the American Chemical Society*, 2009, **131**, 1883.

	α (°) 90.00 β (°) 90.00 γ (°) 90.00		
Catena-[(μ_6-Benzene-1,3,5-tricarboxylato)-tris(μ_2-formato-O,O')-tris(dimethylformamide-O)-tri-nickel(ii)]	Space Group: P -3 a (Å) 13.823 b (Å) 13.823 c (Å) 7.9625 α (°) 90.00 β (°) 90.00 γ (°) 120.00	802890	*Inorganic Chemistry*, 2011, **50**, 5085-5097.
$[Co_3Ni_3(BTC^{3-})_2(HCOO^-)_6(DMF)_6]$	Space Group: P -3 a (Å) 13.908 b (Å) 13.908 c (Å) 8.0810 α (°) 90.00 β (°) 90.00 γ (°) 120.00	2517104	This Work

Table S6: ICP-OES results of NCBMOF-11, NCBMOF-12, and NCBMOF-21.

Sample name	Ni content (ppm)	Co content (ppm)	Ni:Co molar ratio
NCBMOF-11	7.524796289	7.245974552	1:1.04
NCBMOF-12	5.094065209	9.444368253	1:1.85
NCBMOF-21	8.874164224	4.385581907	2:0.98

Table S7: Rietveld refinement parameters of NCBMOF@PBA-21 and AlVO.

NCBMOF@PBA-21	AlVO
Space group: *P 21/c* a = 7.20(1) Å b = 7.23(1) Å c = 12.78(2) Å α = 90.00(0)° β = 122.76(13)° γ = 90.00(0)° WR_P = 7.41%	Space group: *P -1* a = 10.836(2) Å b = 9.514(3) Å c = 14.104(3) Å α = 92.31(2)° β = 91.14(2)° γ = 86.22(3)° WR_P = 4.30%

Rp = 5.79% χ^2 = 0.81	R_p = 3.26% χ^2 = 0.86

Table S8: R_S and R_{CT} data of NCBMOF-12 and NCBMOF@PBA-12 positive electrodes at before and after cycling test.

	NCBMOF-12		**NCBMOF@PBA-12**	
	Before	After	Before	After
R_S [Ω]	6	6	6	6
R_{CT} [Ω]	10	60	2	2.5

Table S9: R_S and R_{CT} data of AlVO and AlVO@C negative electrodes at before and after cycling test.

	AlVO		**AlVO@C**	
	Before	After	Before	After
R_S [Ω]	6	6	6	6
R_{CT} [Ω]	13	72	8	9.5

Table S10: R_S and R_{CT} data of NCBMOF@PBA-12//AlVO@C full cells at before and after cycling test.

	Cycling within 0-1.2 V		**Cycling within 0-1.5 V**		**Cycling within 0-1.8 V**	
	Before	After	Before	After	Before	After
R_S [Ω]	0.96	0.96	0.97	0.97	1.17	1.17
R_{CT} [Ω]	1.74	2.15	1.73	2.12	2.04	4.06

Supporting Figures

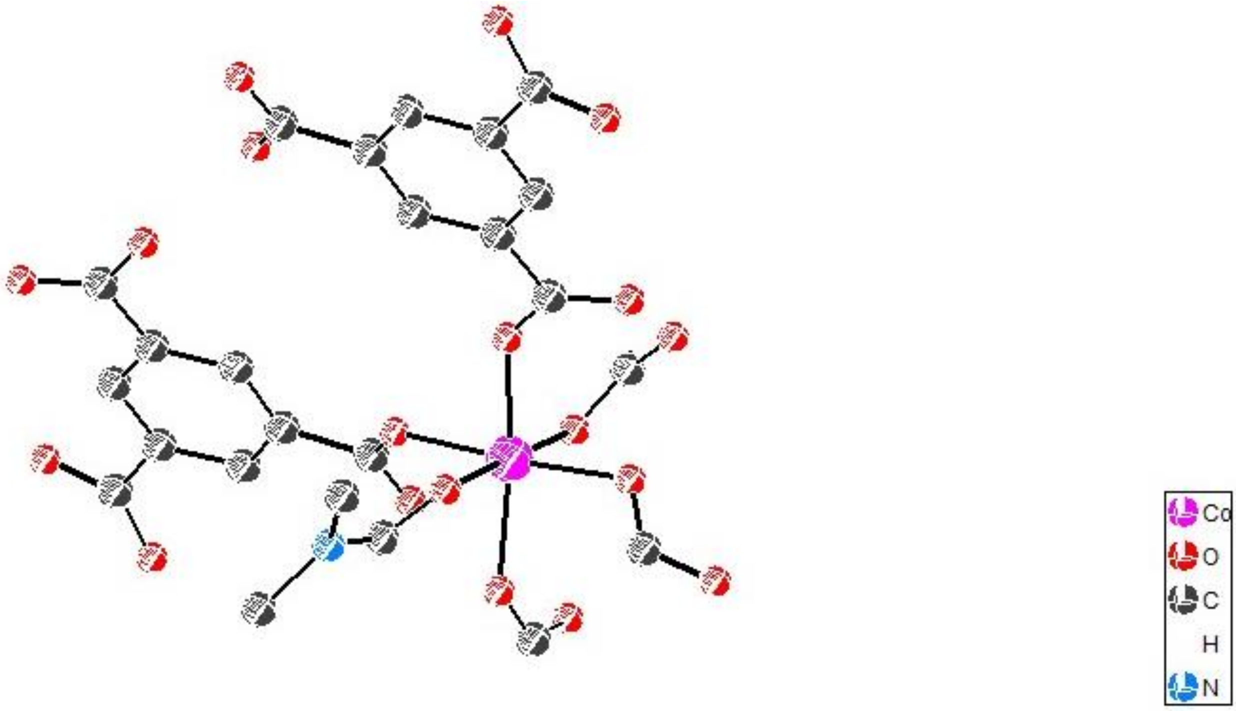

Figure S1. Asymmetric unit of NCBMOF-11.

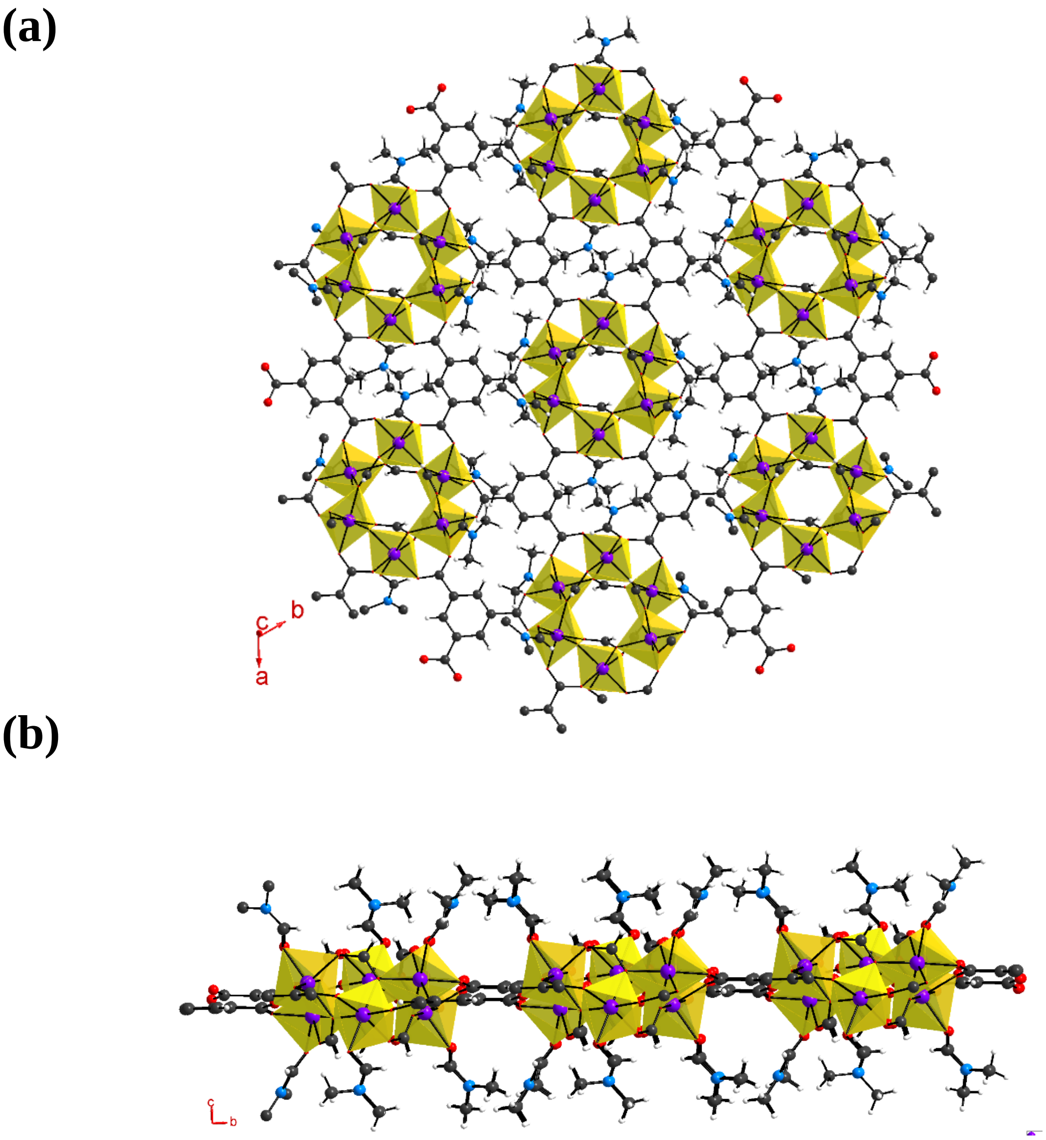

Figure S2: (a) 2D layer and (b) view of 2D layers along the crystallographic *a*-axis of NCBMOF-11.

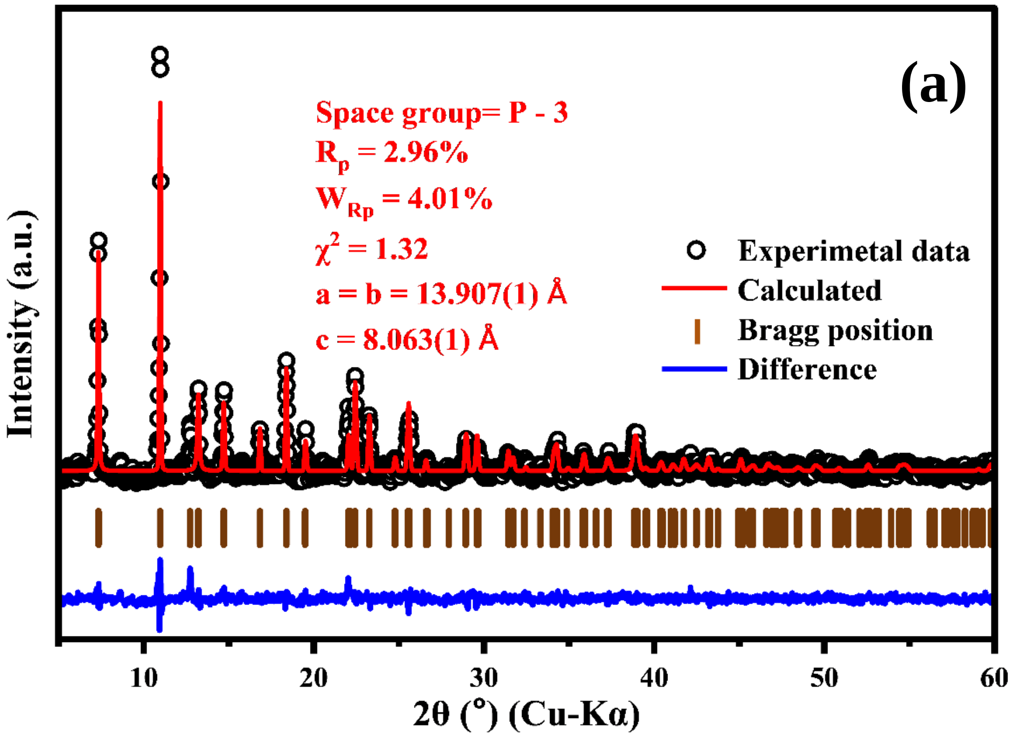

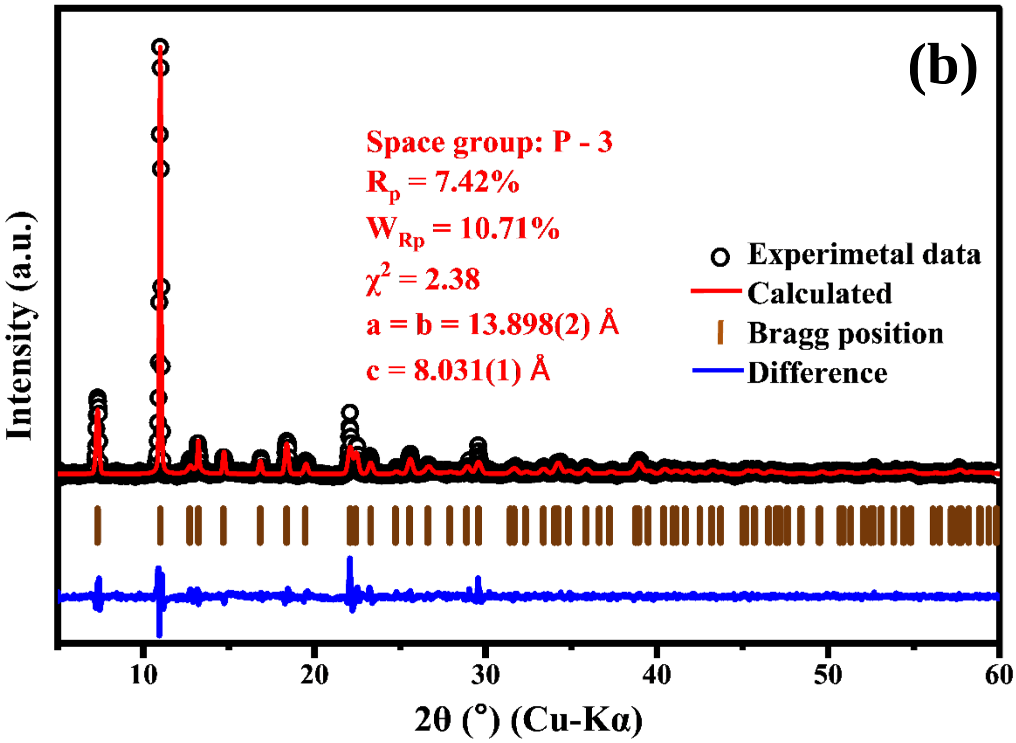

Figure S3: PXRD refinement plot of (a) NCBMOF-11 and (b) NCBMOF-21.

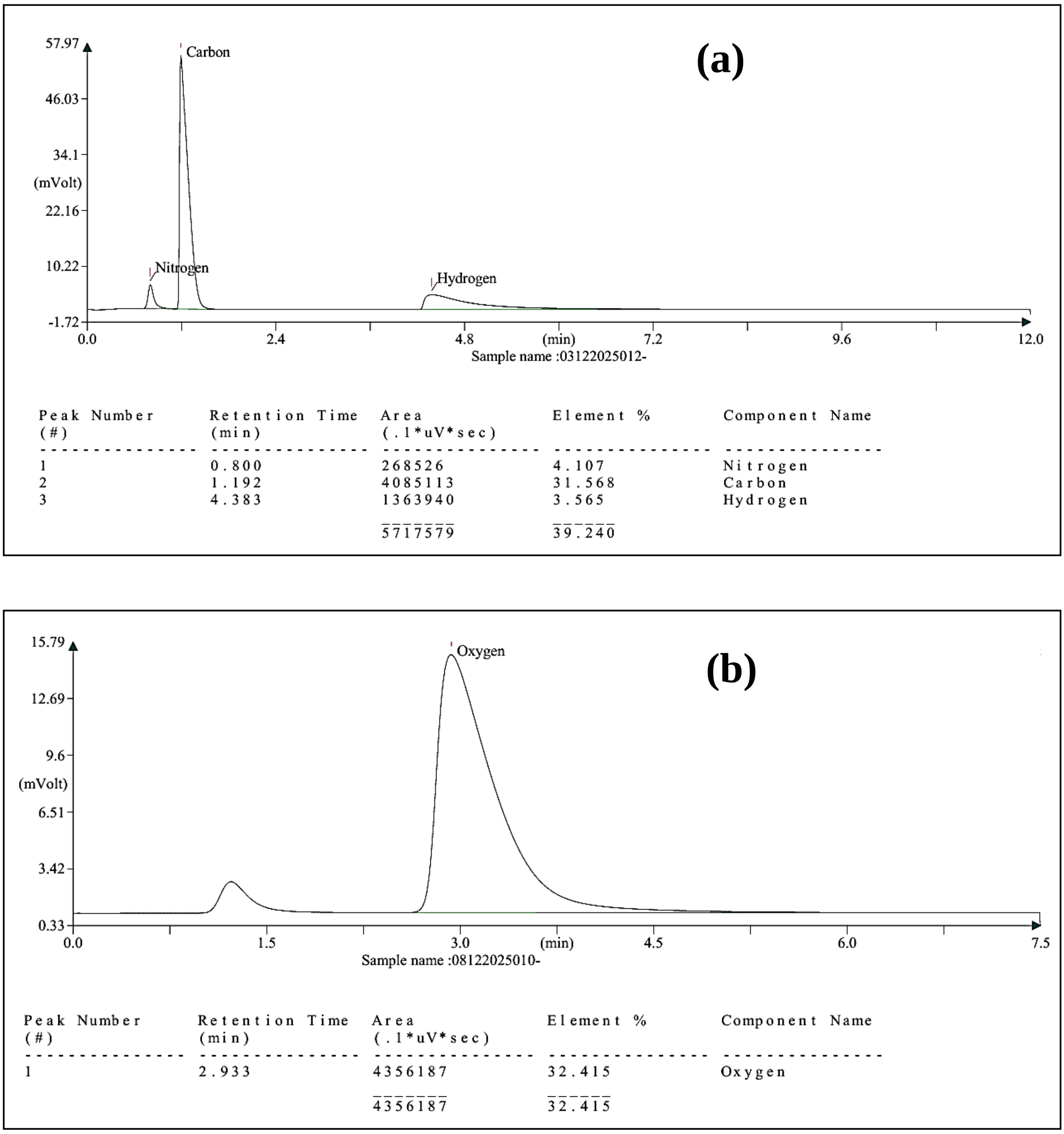

```
Peak Number       Retention Time    Area              Element %         Component Name
(#)               (min)             (.1*uV*sec)
---------------   ---------------   ---------------   ---------------   ---------------
1                 0.800             268526            4.107             Nitrogen
2                 1.192             4085113           31.568            Carbon
3                 4.383             1363940           3.565             Hydrogen
                                    -------           ------
                                    5717579           39.240
```

```
Peak Number       Retention Time    Area              Element %         Component Name
(#)               (min)             (.1*uV*sec)
---------------   ---------------   ---------------   ---------------   ---------------
1                 2.933             4356187           32.415            Oxygen
                                    -------           ------
                                    4356187           32.415
```

Figure S4: (a) CHNS and (b) oxygen analysis data of NCBMOF-11.

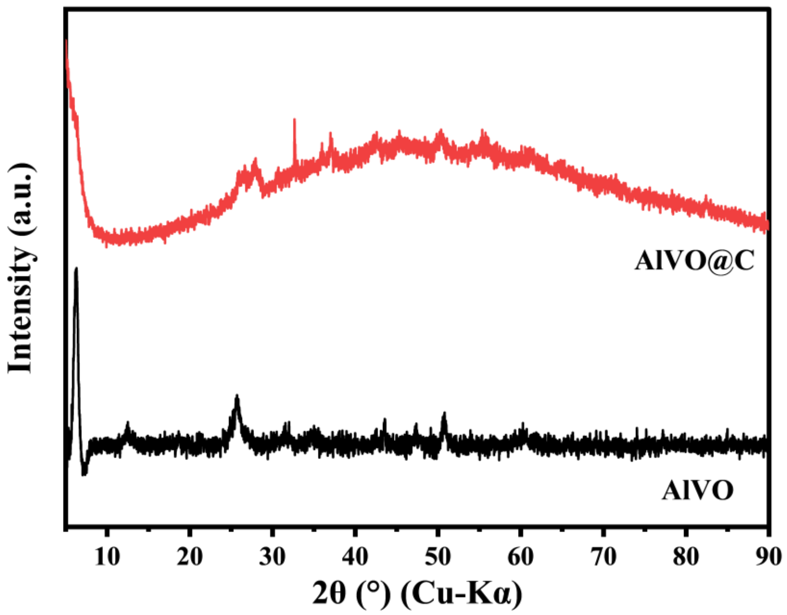

Figure S5: PXRD plots of AlVO and AlVO@C.

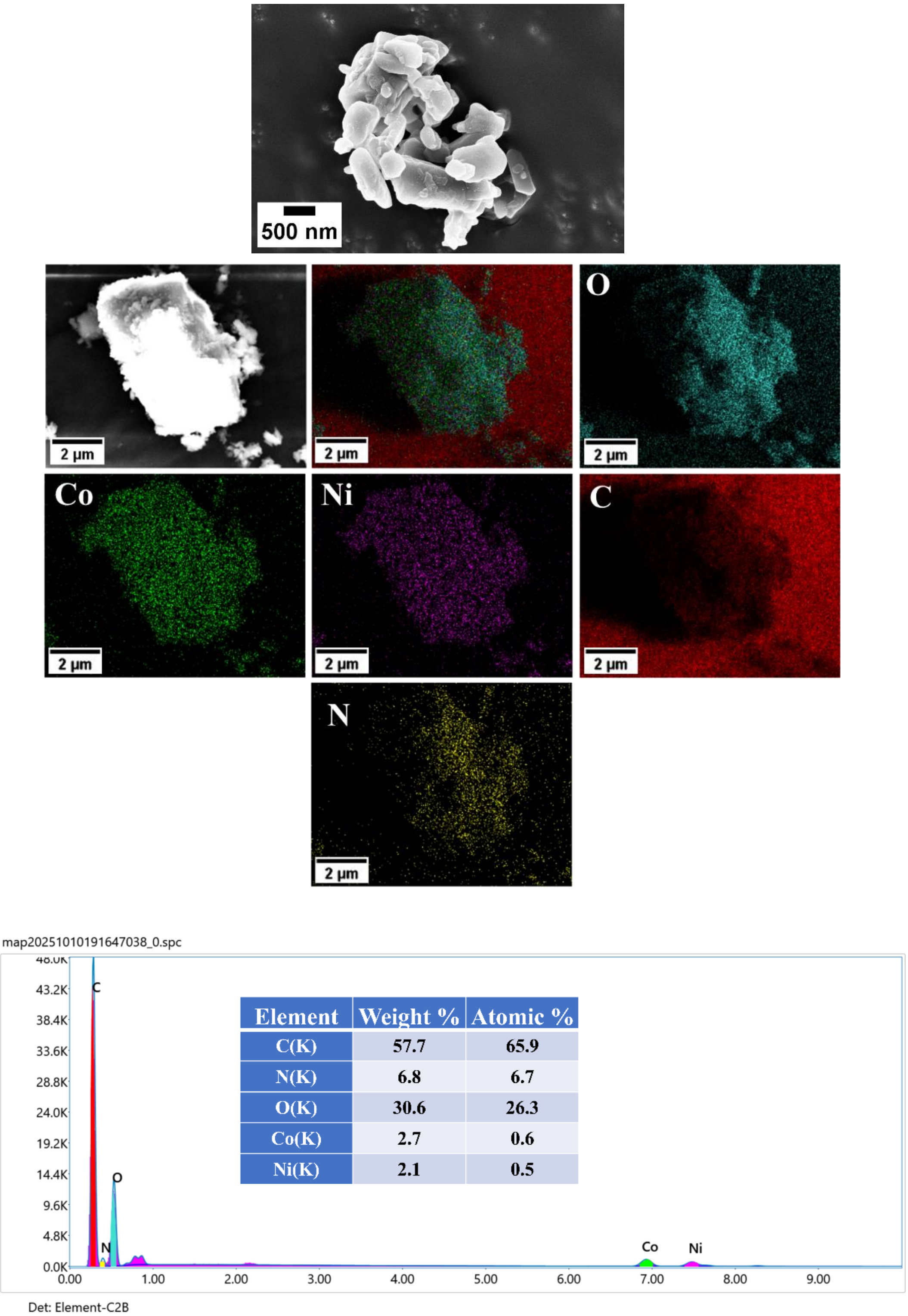

Element	Weight %	Atomic %
C(K)	57.7	65.9
N(K)	6.8	6.7
O(K)	30.6	26.3
Co(K)	2.7	0.6
Ni(K)	2.1	0.5

Figure S6: FESEM-EDX data of NCBMOF-11.

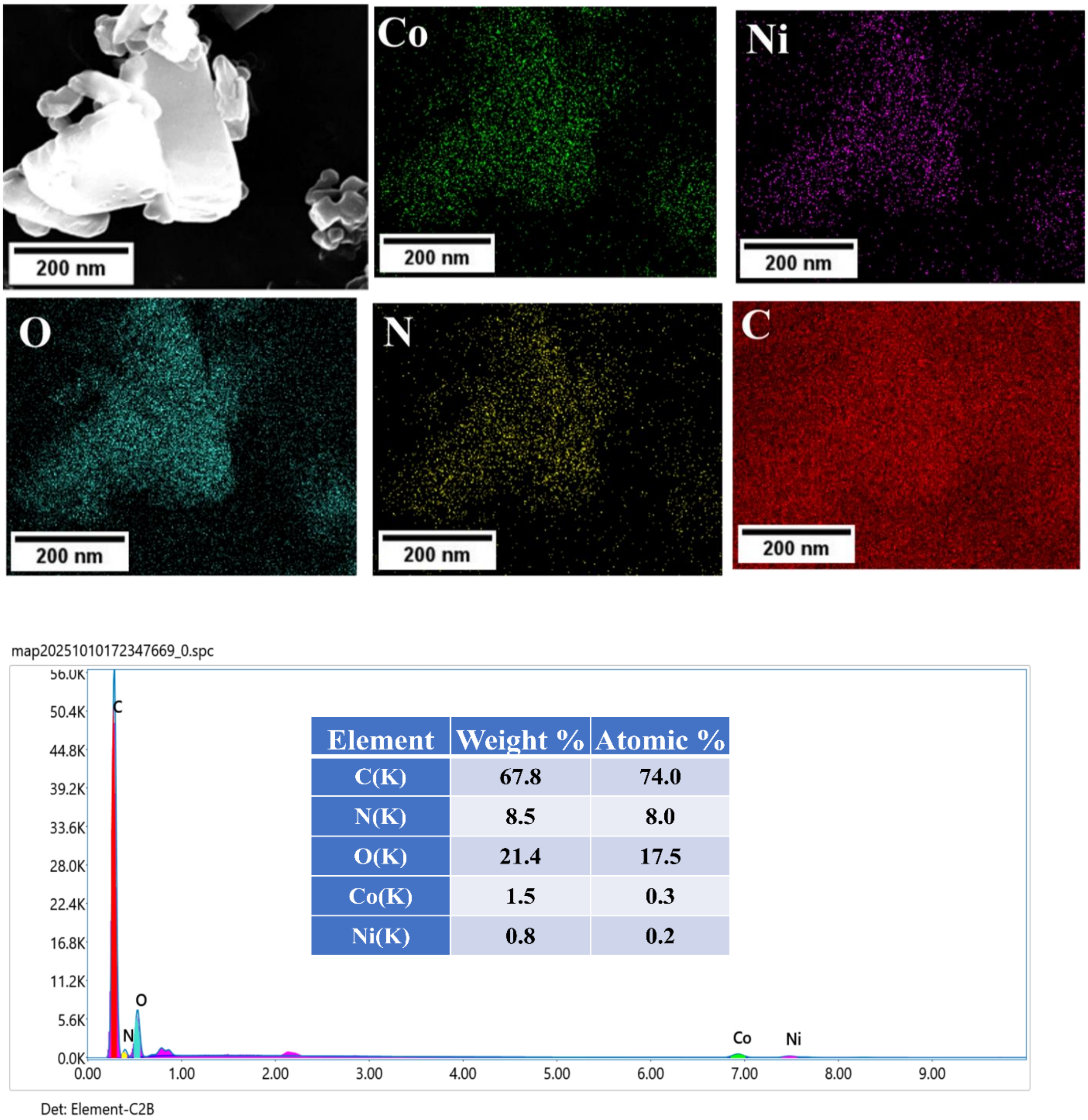

Element	Weight %	Atomic %
C(K)	67.8	74.0
N(K)	8.5	8.0
O(K)	21.4	17.5
Co(K)	1.5	0.3
Ni(K)	0.8	0.2

Figure S7: FESEM-EDX data of NCBMOF-12.-

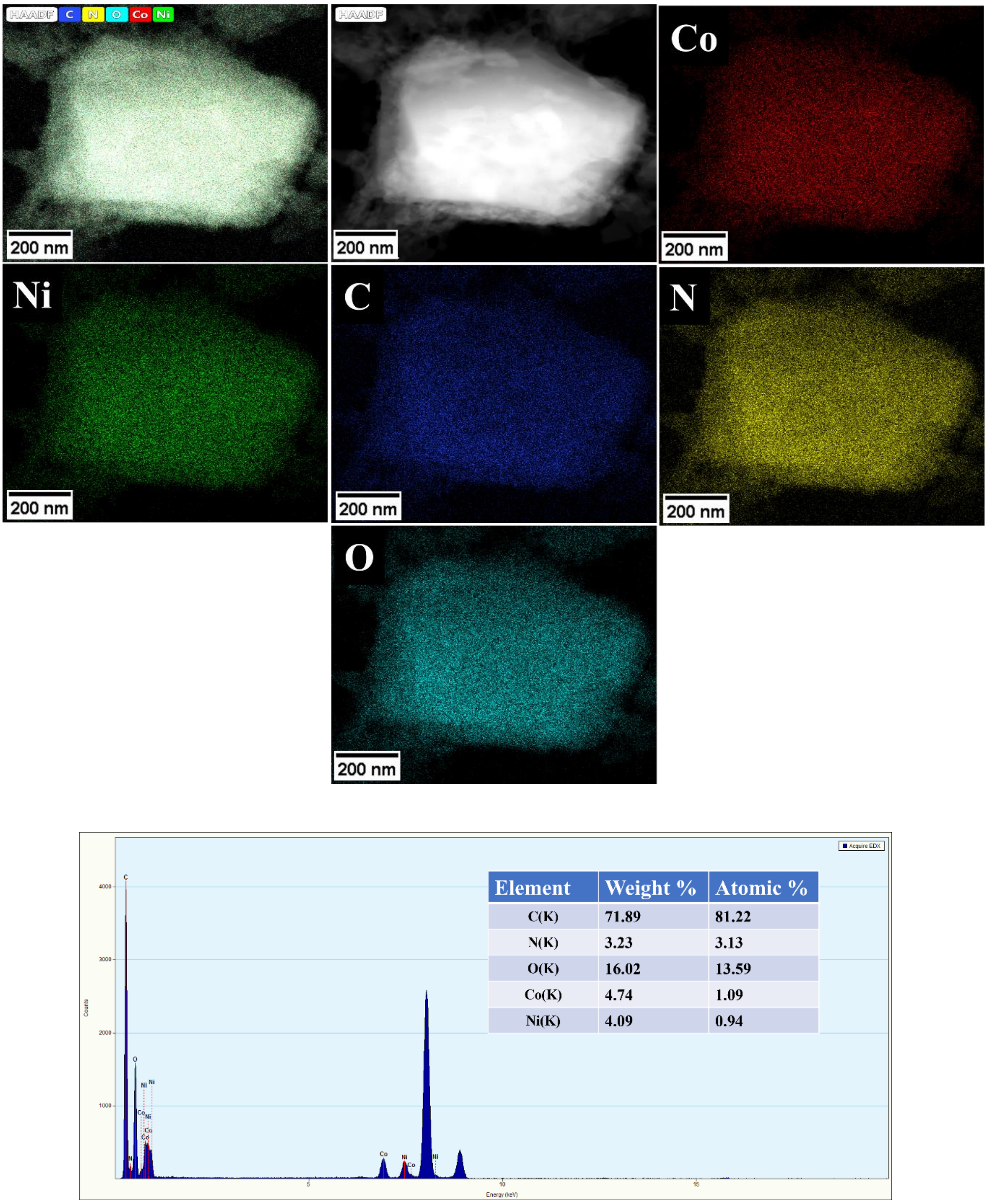

Element	Weight %	Atomic %
C(K)	71.89	81.22
N(K)	3.23	3.13
O(K)	16.02	13.59
Co(K)	4.74	1.09
Ni(K)	4.09	0.94

Figure S8: HAADF-STEM EDX data of NCBMOF-12.

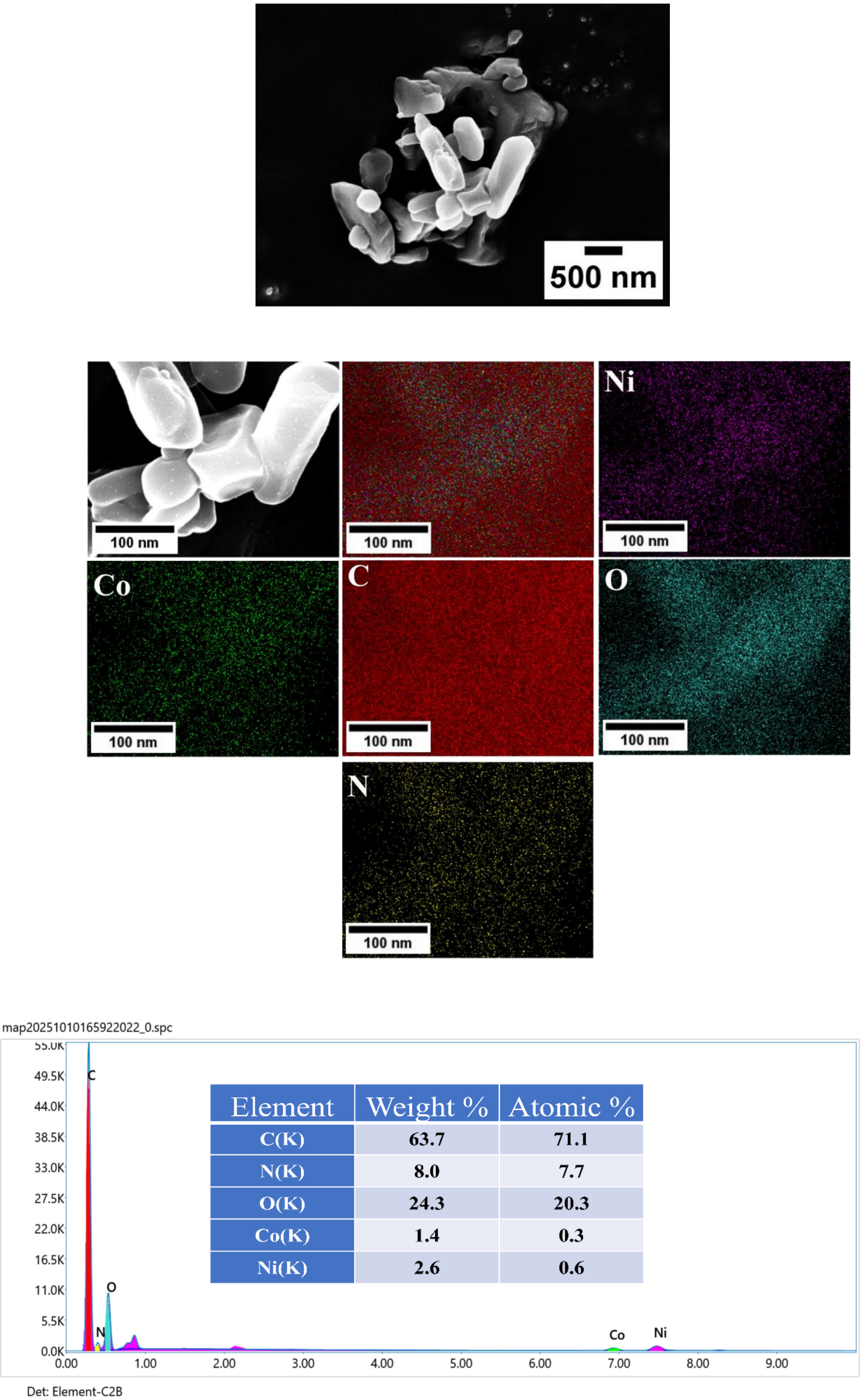

Element	Weight %	Atomic %
C(K)	63.7	71.1
N(K)	8.0	7.7
O(K)	24.3	20.3
Co(K)	1.4	0.3
Ni(K)	2.6	0.6

Figure S9: FESEM-EDX data of NCBMOF-21.

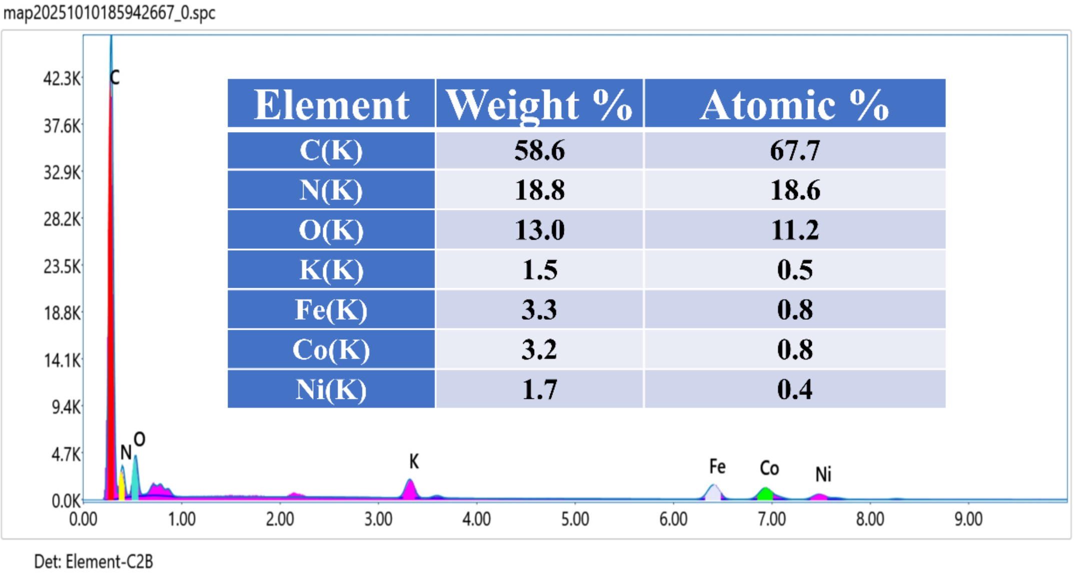

Element	Weight %	Atomic %
C(K)	58.6	67.7
N(K)	18.8	18.6
O(K)	13.0	11.2
K(K)	1.5	0.5
Fe(K)	3.3	0.8
Co(K)	3.2	0.8
Ni(K)	1.7	0.4

Figure S10: FESEM-EDX data of NCBMOF@PBA-12.

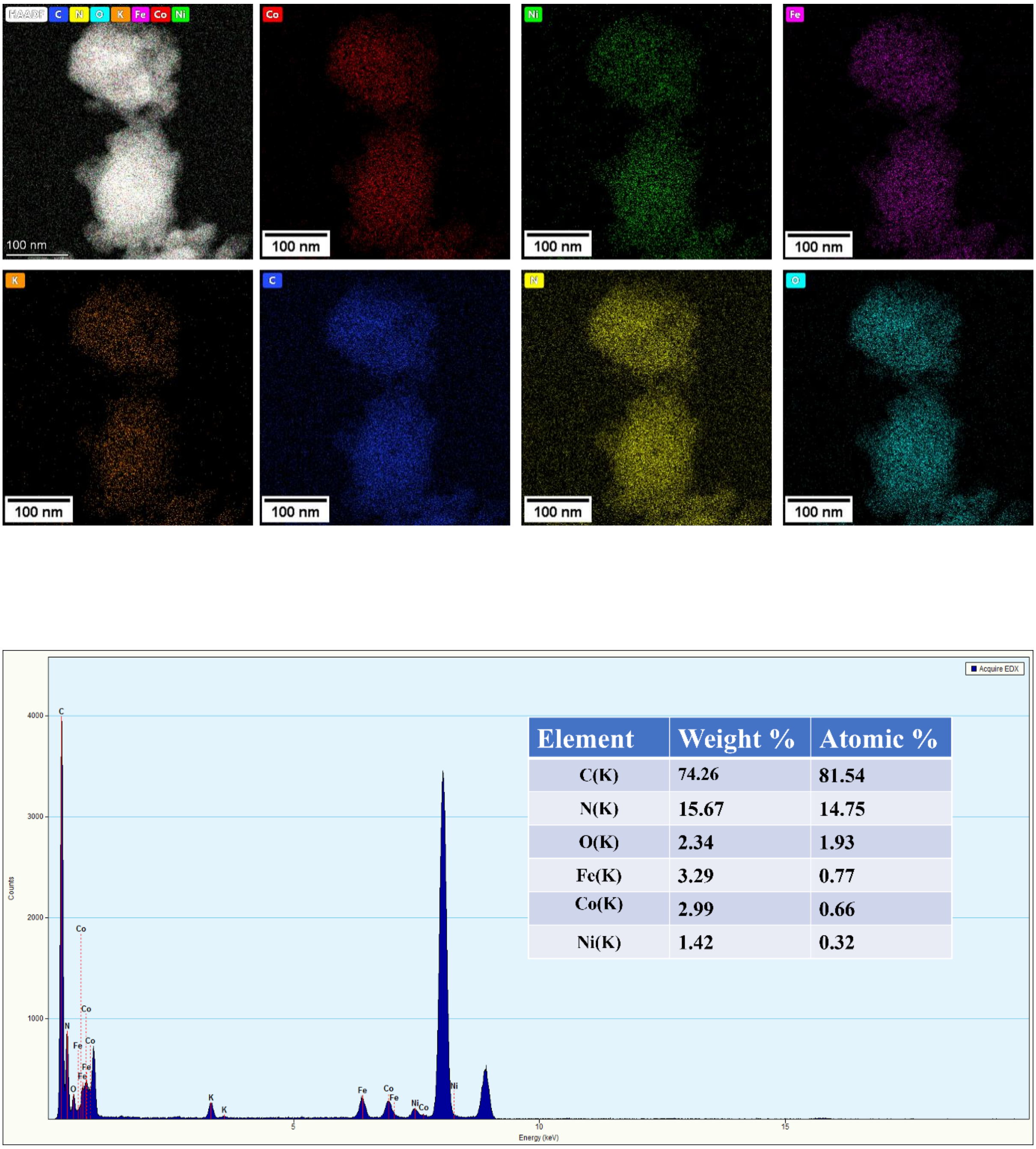

Element	Weight %	Atomic %
C(K)	74.26	81.54
N(K)	15.67	14.75
O(K)	2.34	1.93
Fe(K)	3.29	0.77
Co(K)	2.99	0.66
Ni(K)	1.42	0.32

Figure S11: HAADF-STEM EDX data of NCBMOF@PBA-12.

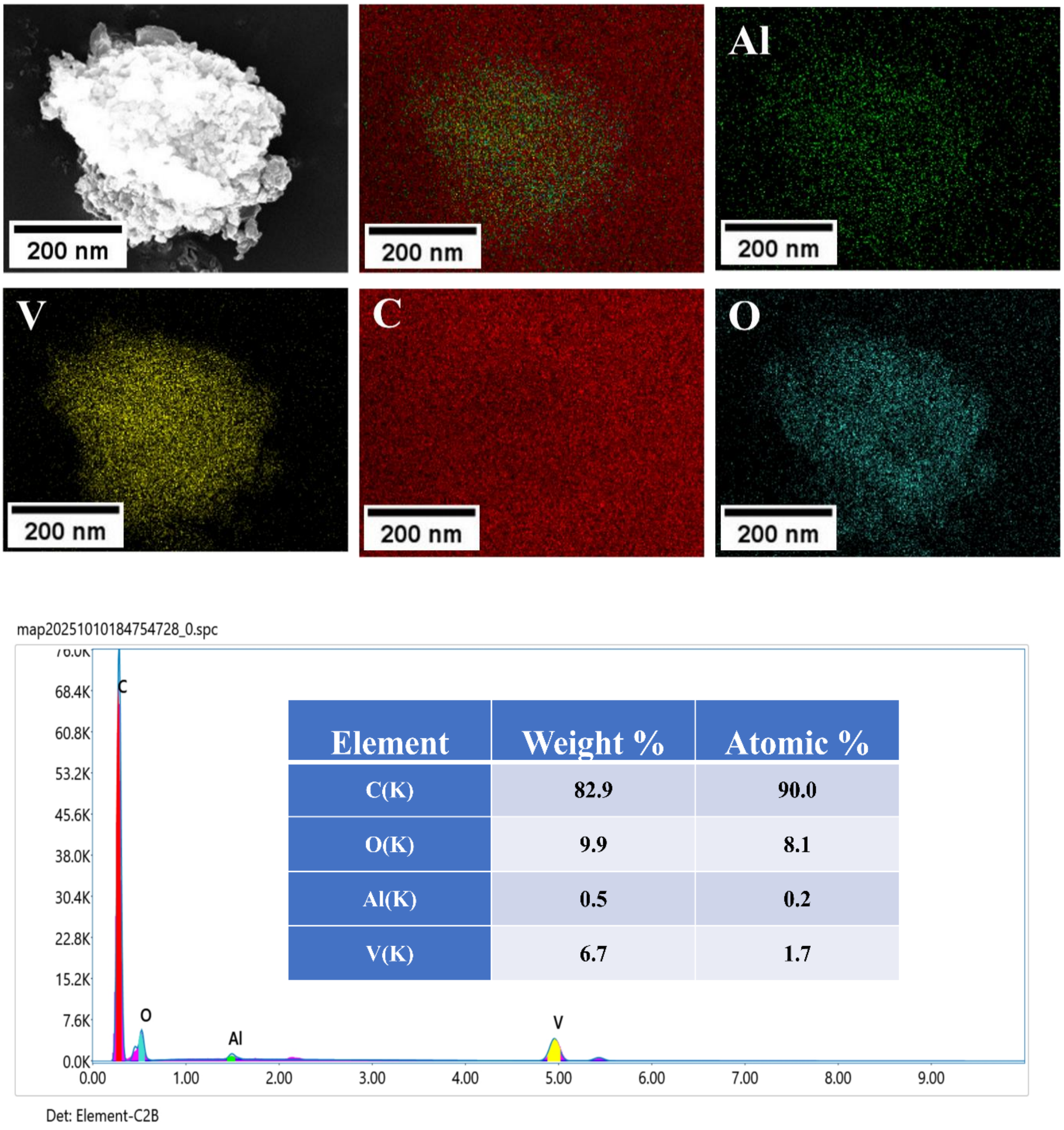

Element	Weight %	Atomic %
C(K)	82.9	90.0
O(K)	9.9	8.1
Al(K)	0.5	0.2
V(K)	6.7	1.7

Figure S12: FESEM-EDX data of AlVO.

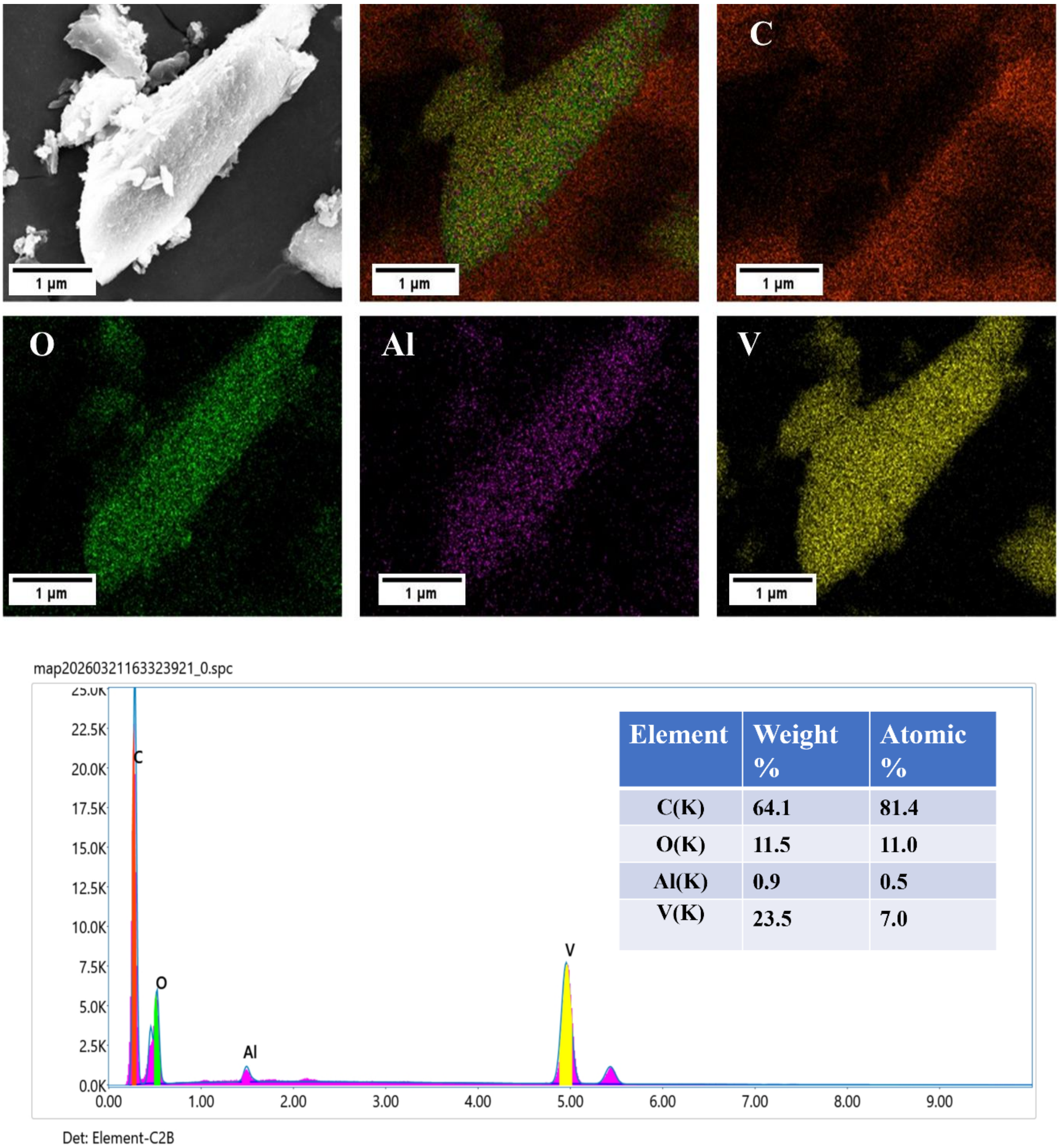

Element	Weight %	Atomic %
C(K)	64.1	81.4
O(K)	11.5	11.0
Al(K)	0.9	0.5
V(K)	23.5	7.0

Figure S13: FESEM-EDX data of AlVO@C.

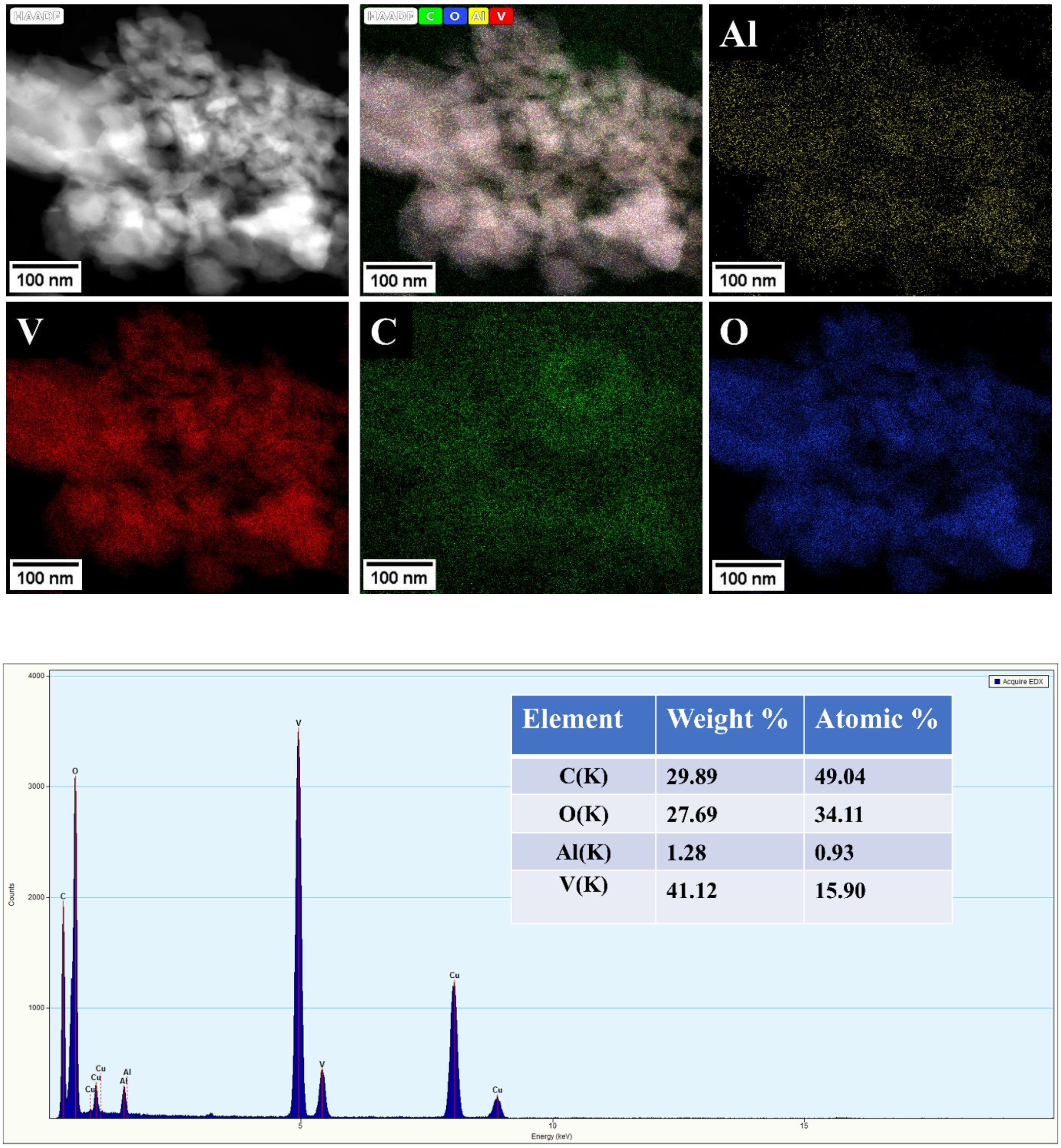

Element	Weight %	Atomic %
C(K)	29.89	49.04
O(K)	27.69	34.11
Al(K)	1.28	0.93
V(K)	41.12	15.90

Figure S14: HAADF-STEM EDX data of AlVO.

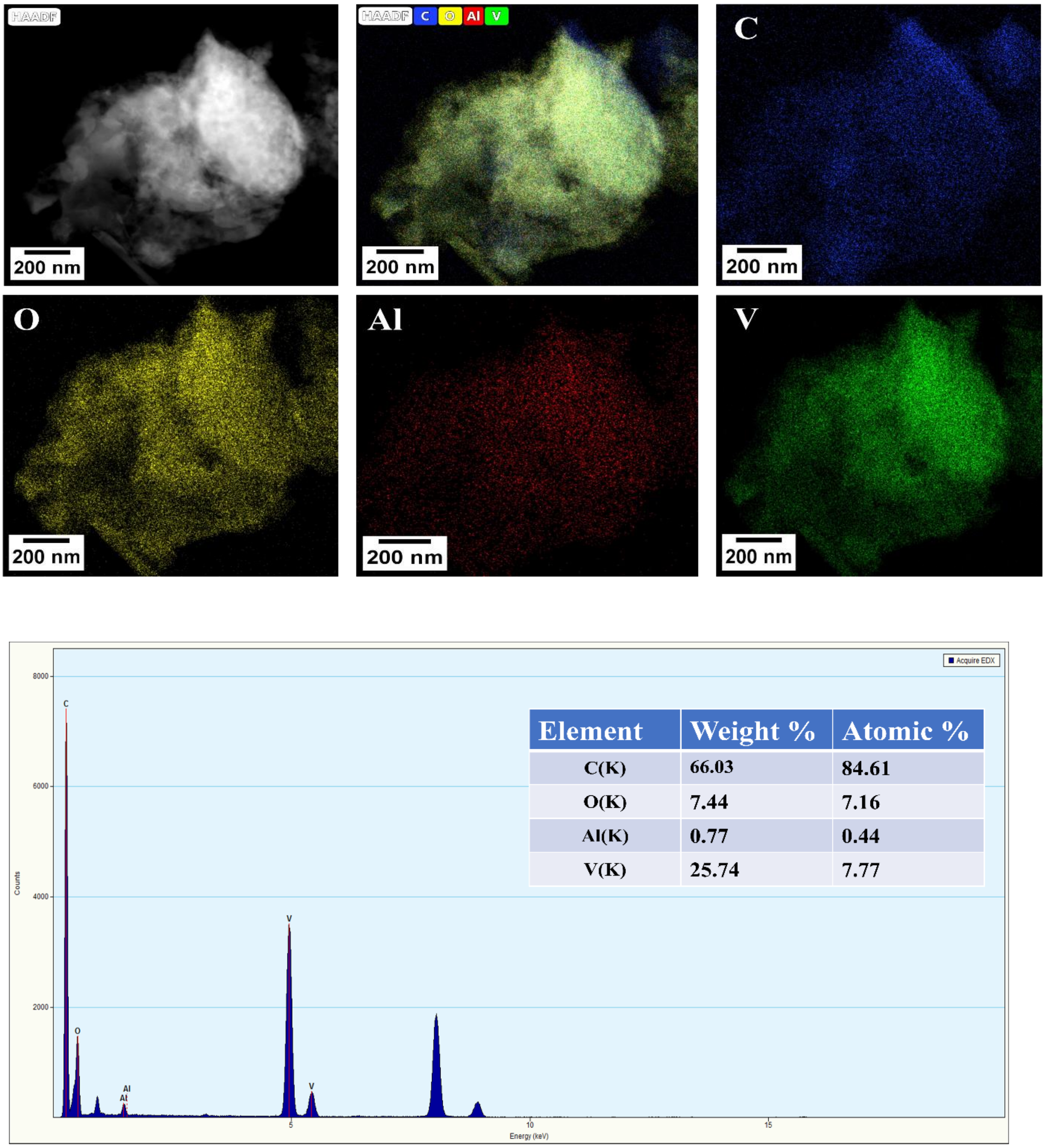

Element	Weight %	Atomic %
C(K)	66.03	84.61
O(K)	7.44	7.16
Al(K)	0.77	0.44
V(K)	25.74	7.77

Figure S15: HAADF-STEM EDX data of AlVO@C.

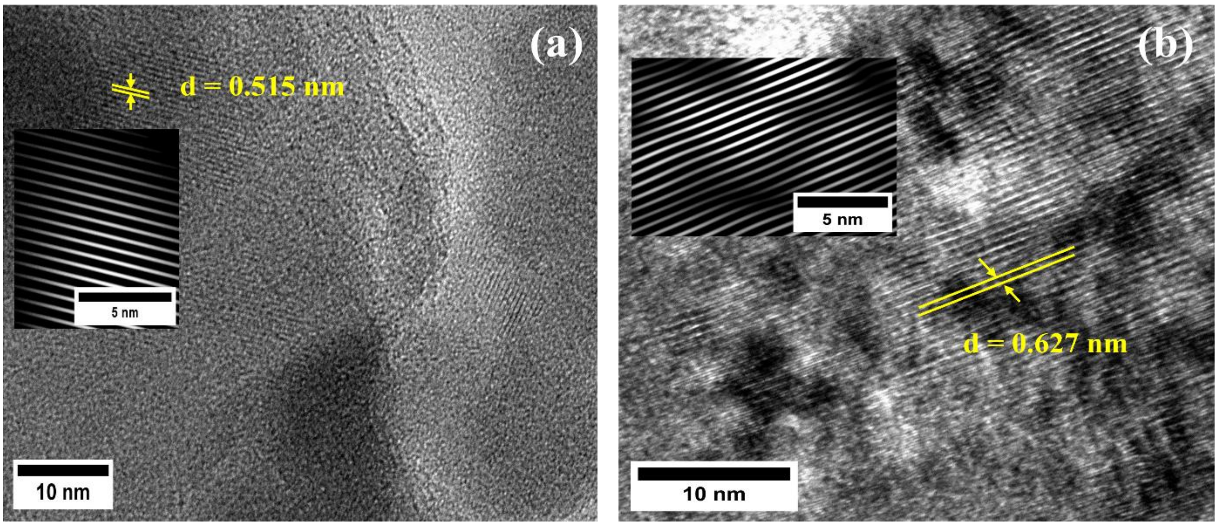

Figure S16: HRTEM images showing lattice fringes: (a) NCBMOF@PBA-12 and (b) AlVO@C.

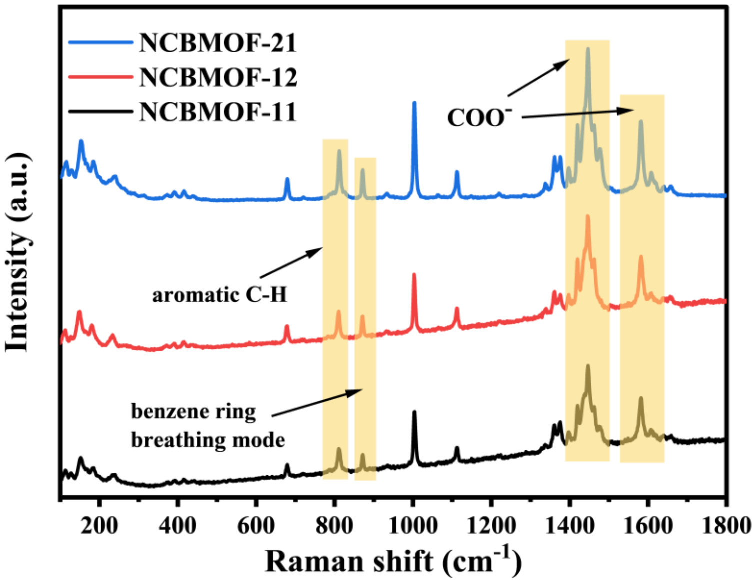

Figure S17: Raman spectra of NCBMOF-11, NCBMOF-12 and NCBMOF-21.

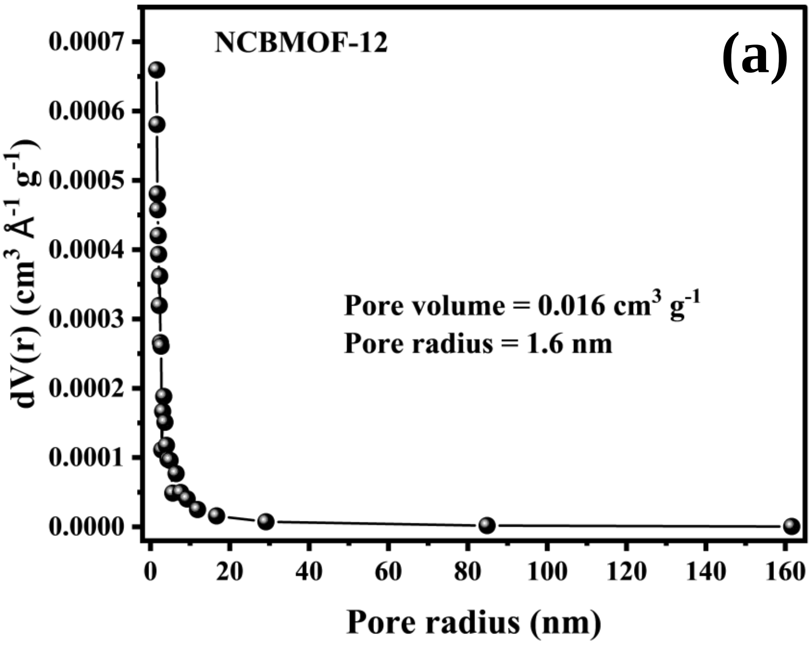

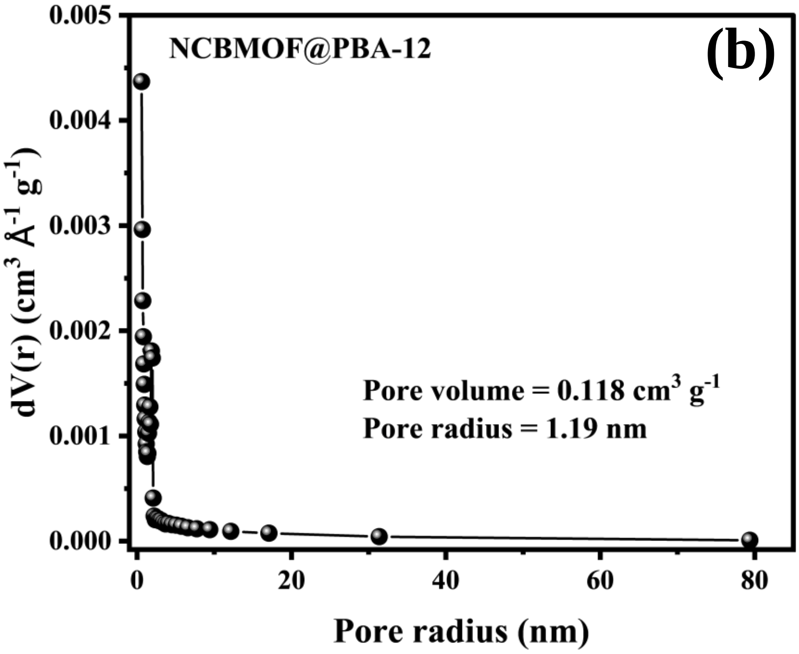

Figure S18: Pore size distribution plots of (a) NCBMOF-12 and (b) NCBMOF@PBA-12.

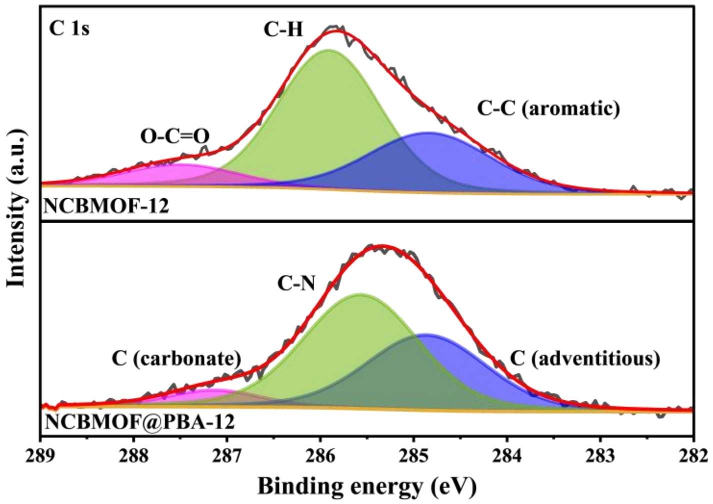

Figure S19: C 1s deconvoluted spectra of NCBMOF-12 and NCBMOF@PBA-12.

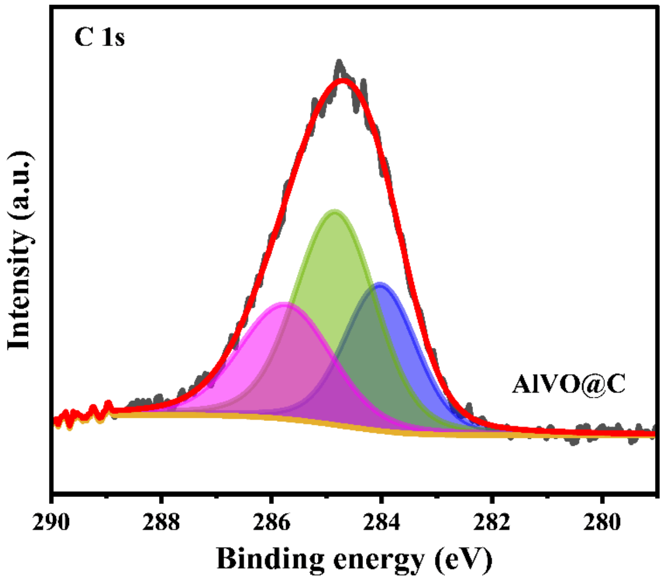

Figure S20: C 1s deconvoluted spectra of AlVO@C.

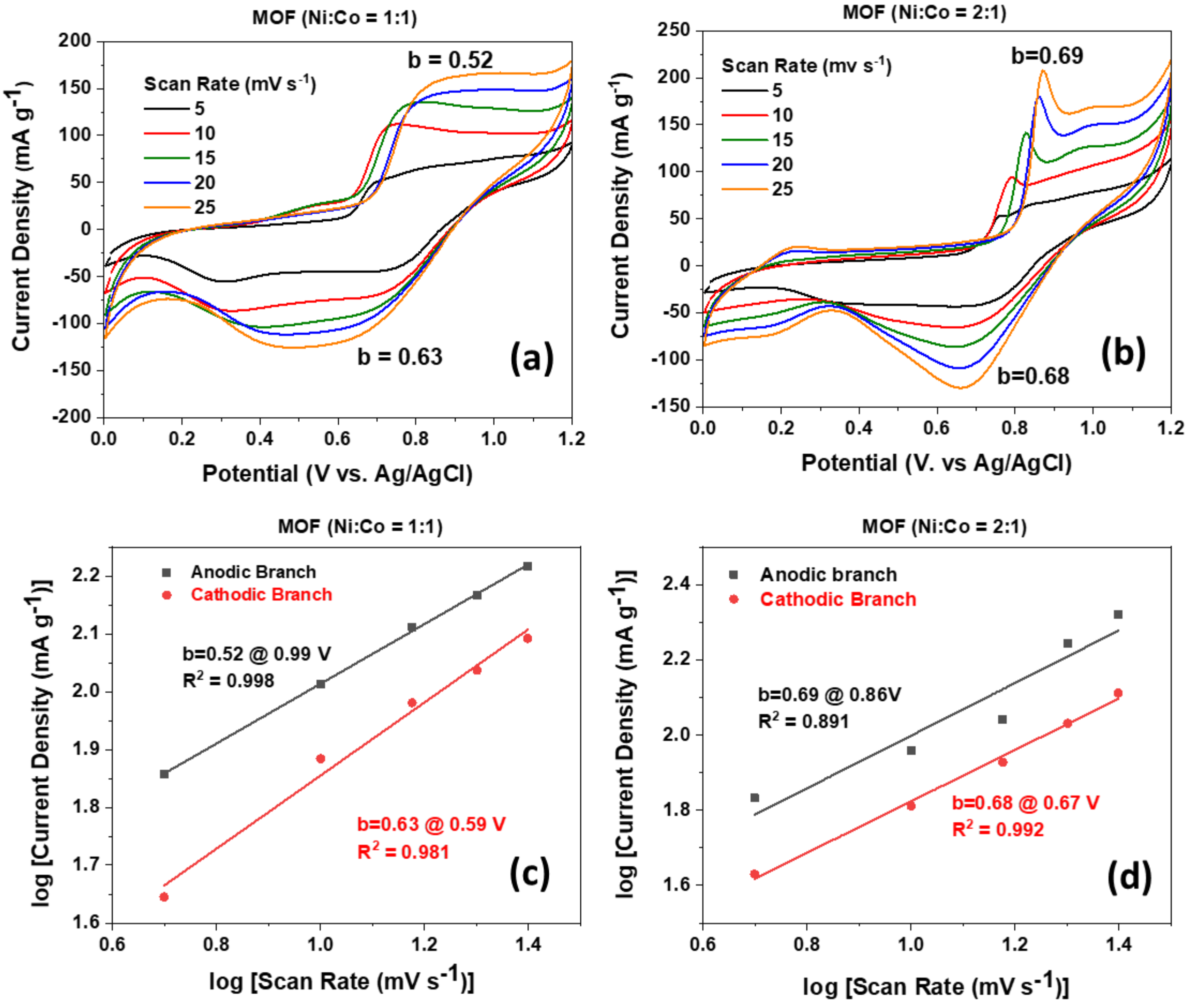

Figure S21: CV of (a) NCBMOF-11, (b) NCBMOF-21; b-value calculation of (c) NCBMOF-11, (d) NCBMOF-21.

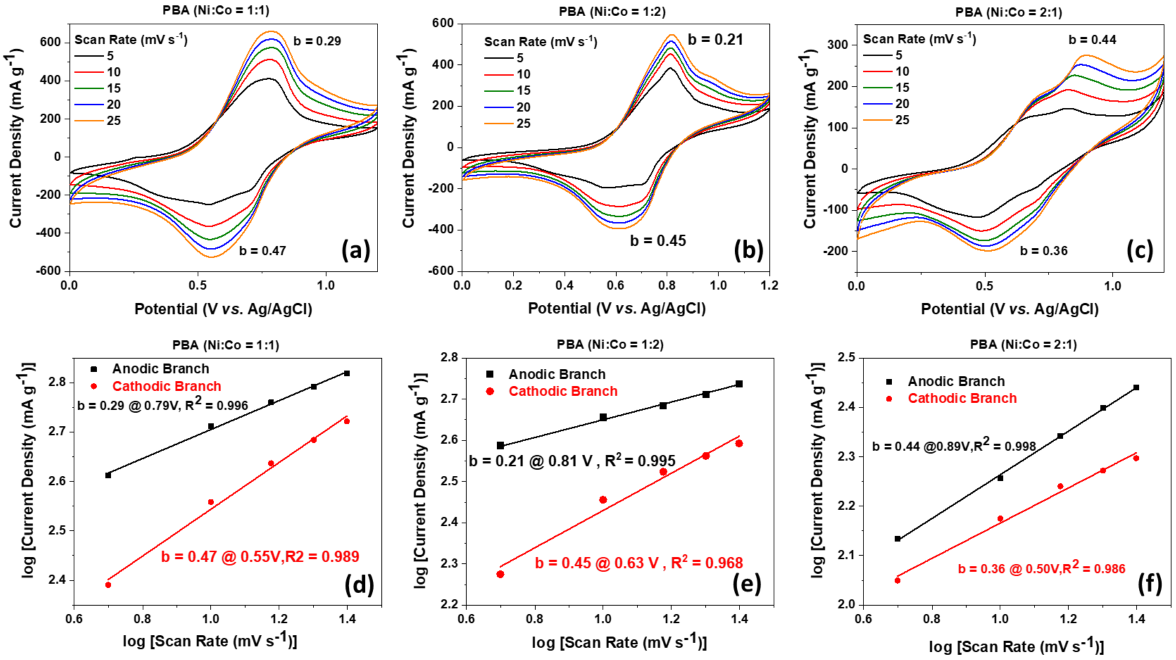

Figure S22: CV profiles of (a) PBA-11, (b) PBA-12, (c) PBA-21; b-value calculations for (d) PBA-11, (e) PBA-12, (f) PBA-21. In general, the b-value (from the relationship $i = a \cdot v^b$) lies between 0.5 (diffusion-controlled process) and 1 (surface-controlled capacitive process). However, values lower than 0.5 can arise under certain non-ideal conditions. In the present case, the low b-values (0.21–0.47) observed for the PBA electrodes indicate a strongly diffusion-limited charge storage process with sluggish ion transport kinetics. [Ref: *Energy & Environmental Science*, 2014, 7, 1597–1614 & *J. Phys. Chem. C*, 2021, 125, 16946–16954]

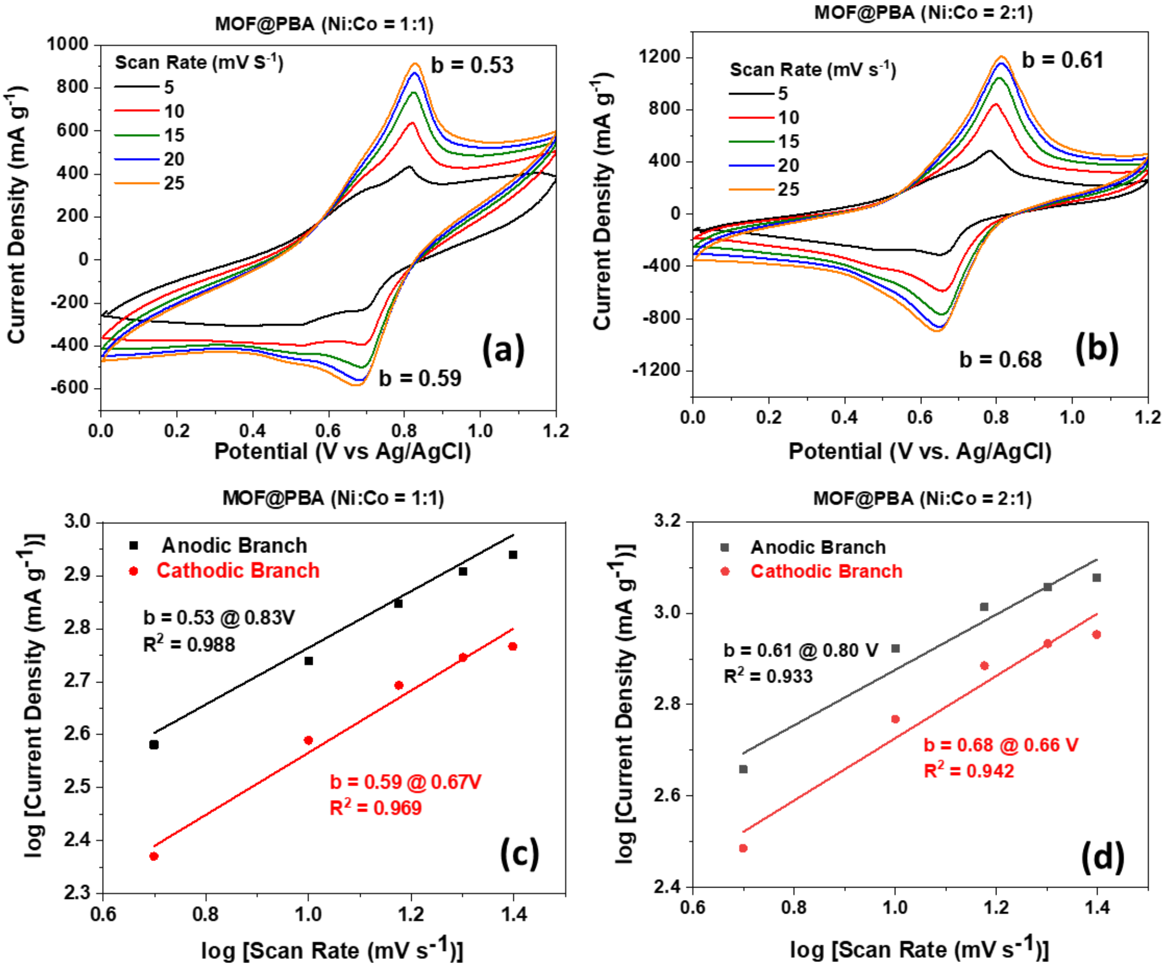

Figure S23: CV of (a) NCBMOF@PBA-11, (b) NCBMOF@PBA-21; b-value calculation of (c) NCBMOF@PBA-11, (d) NCBMOF@PBA-21.

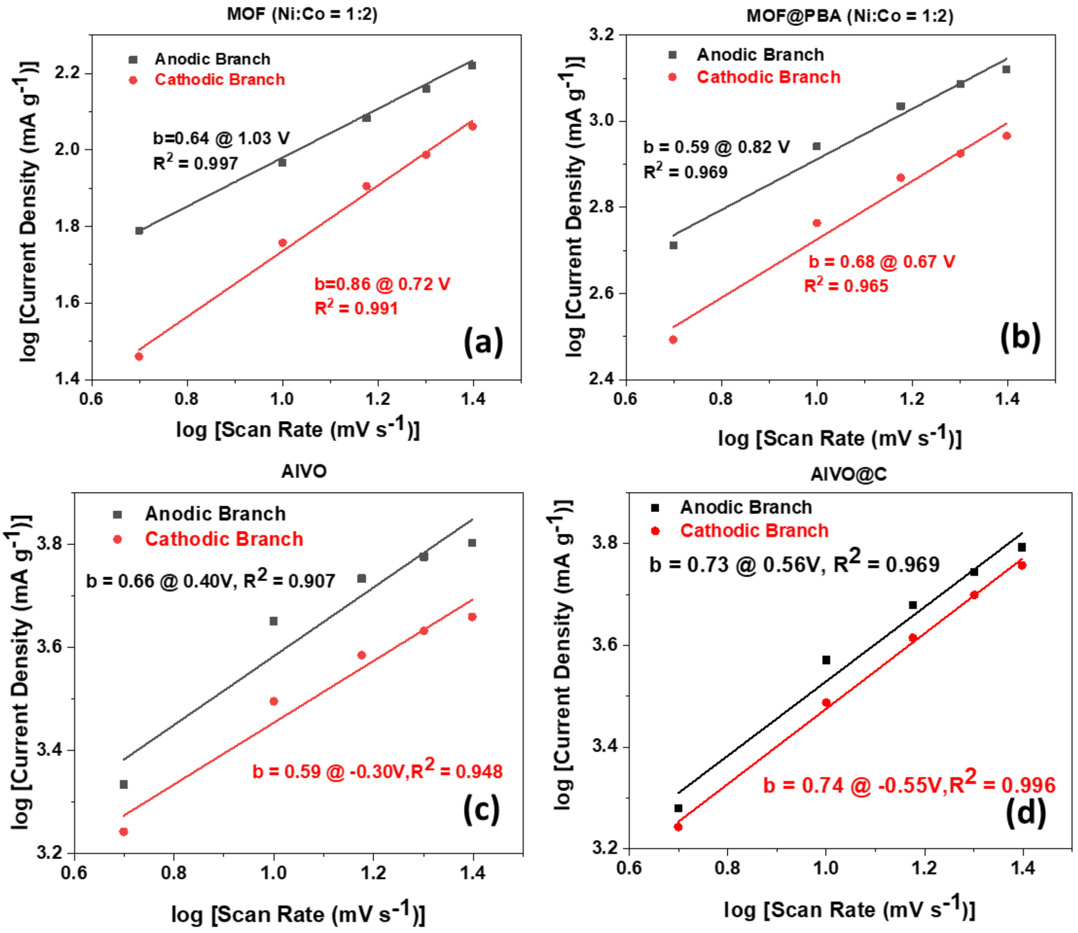

Figure S24: b-value calculation of (a) NCBMOF-12, (b) NCBMOF@PBA-12, (c) AlVO, and (d) AlVO@C.

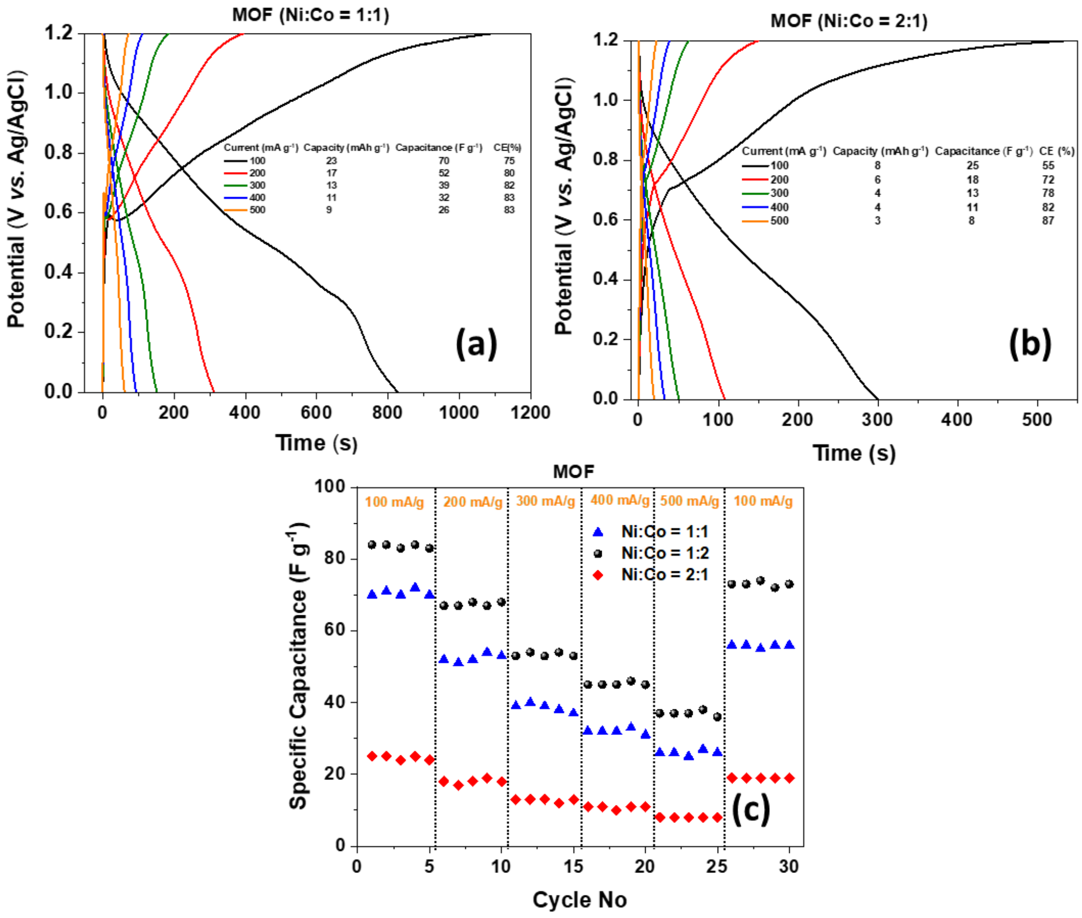

Current (mA g^{-1})	Capacity (mAh g^{-1})	Capacitance (F g^{-1})	CE(%)
100	23	70	75
200	17	52	80
300	13	39	82
400	11	32	83
500	9	26	83

Current (mA g^{-1})	Capacity (mAh g^{-1})	Capacitance (F g^{-1})	CE (%)
100	8	25	55
200	6	18	72
300	4	13	78
400	4	11	82
500	3	8	87

Figure S25: GCD of (a) NCBMOF-11, (b) NCBMOF-21, (c) comparison of rate capability among three compositions namely NCBMOF-11, NCBMOF-12 and NCBMOF-21.

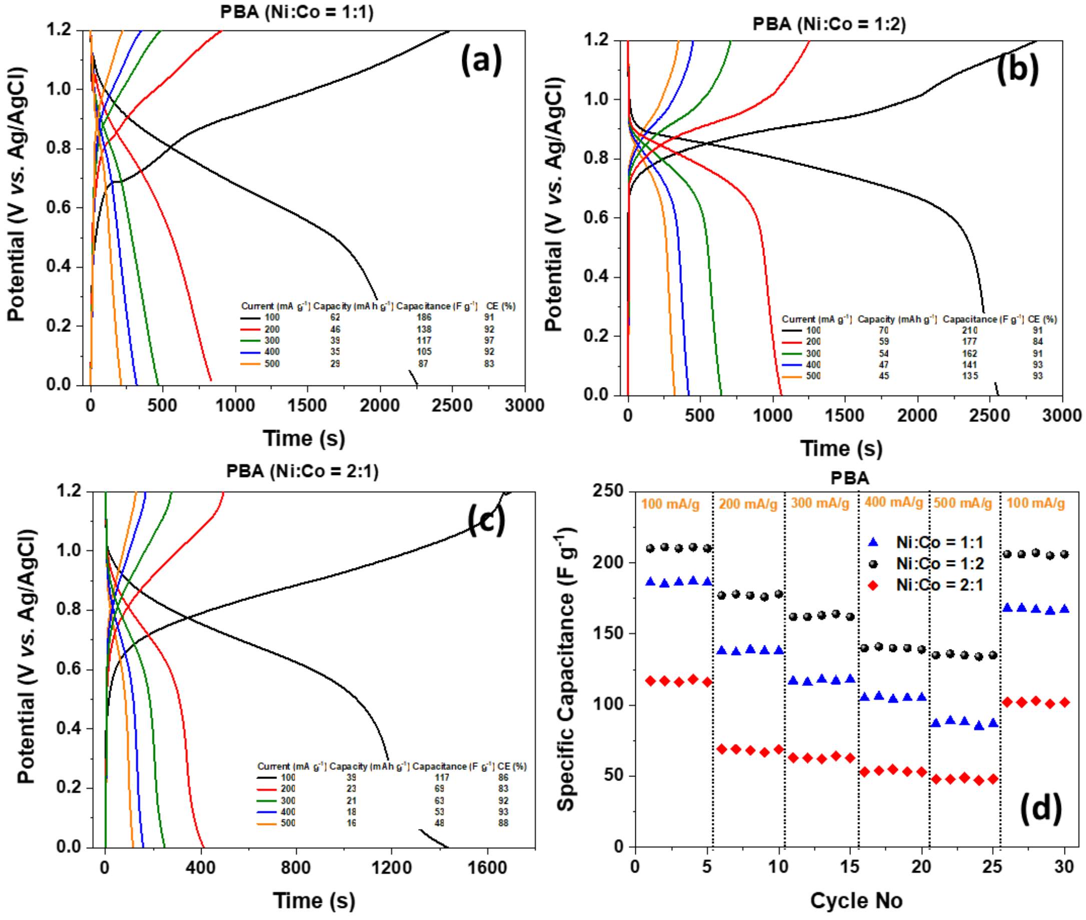

Figure S26: GCD of (a) PBA-11, (b) PBA-12, (c) PBA-21, (d) comparison of rate capability among three compositions.

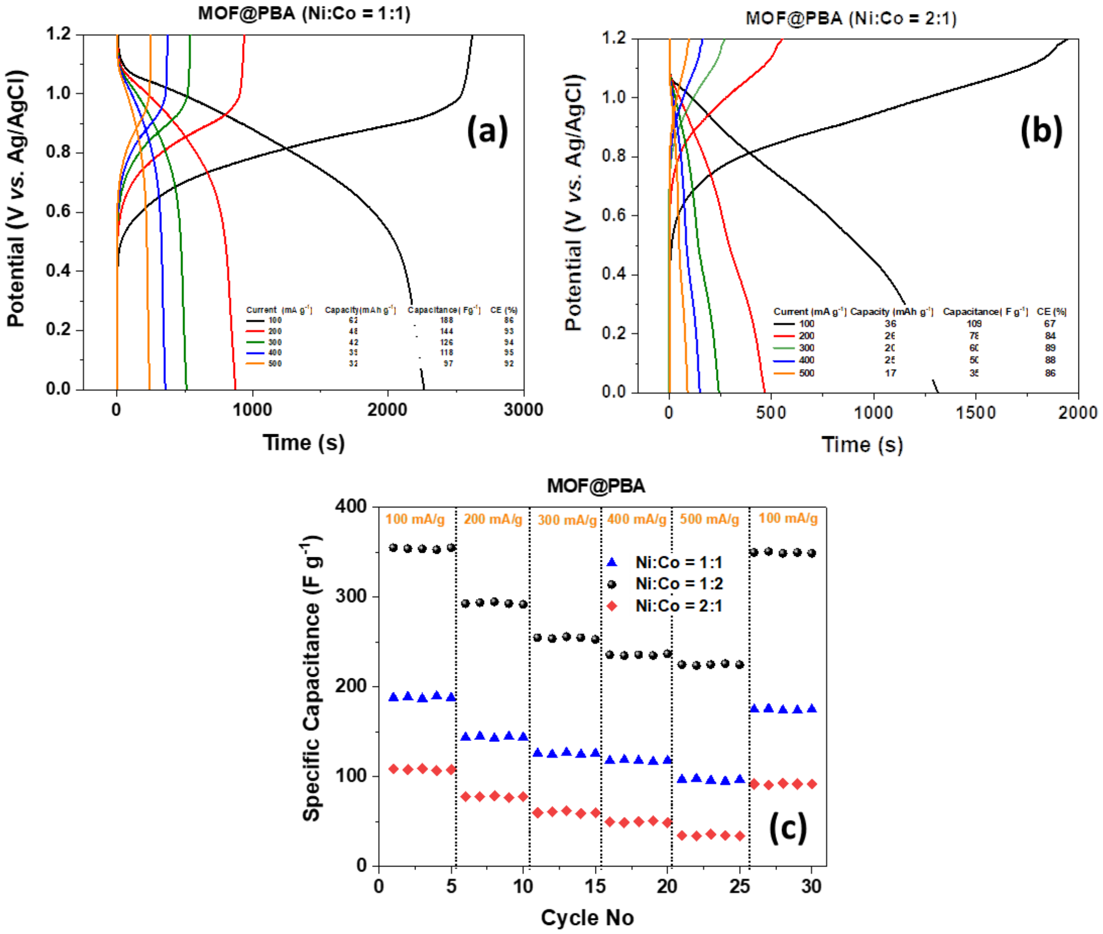

Figure S27: GCD of (a) NCBMOF@PBA-11, (b) NCBMOF@PBA-21, (c) comparison of rate capability among three compositions namely NCBMOF@PBA-11, NCBMOF@PBA-12 and NCBMOF@PBA-21.

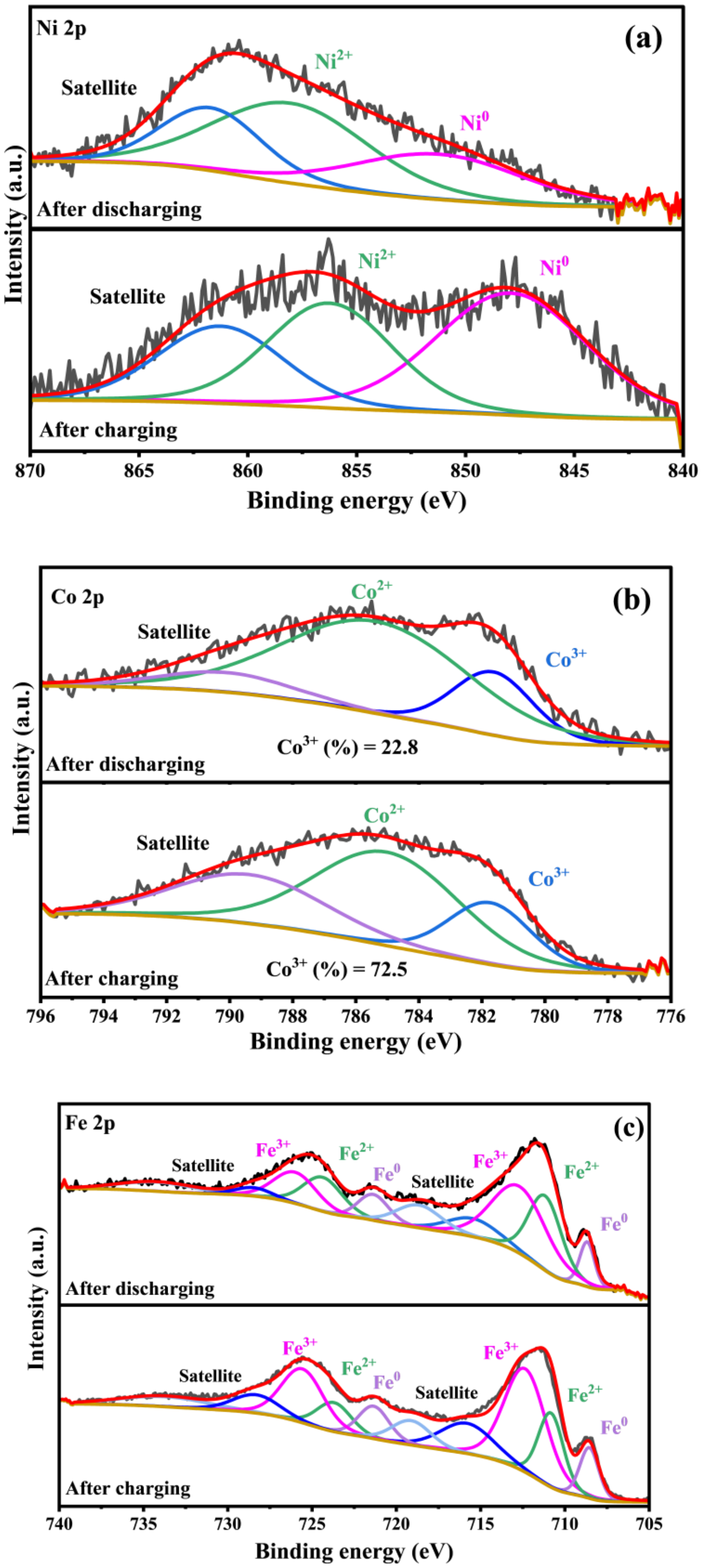

Figure S28: *ex situ* XPS analysis of NCBMOF@PBA-12 at its charged and discharged states: (a) Ni 2p, (b) Co 2p, and (c) Fe 2p spectra. Ni and Fe in metallic states are appeared from the stainless steel current collector.

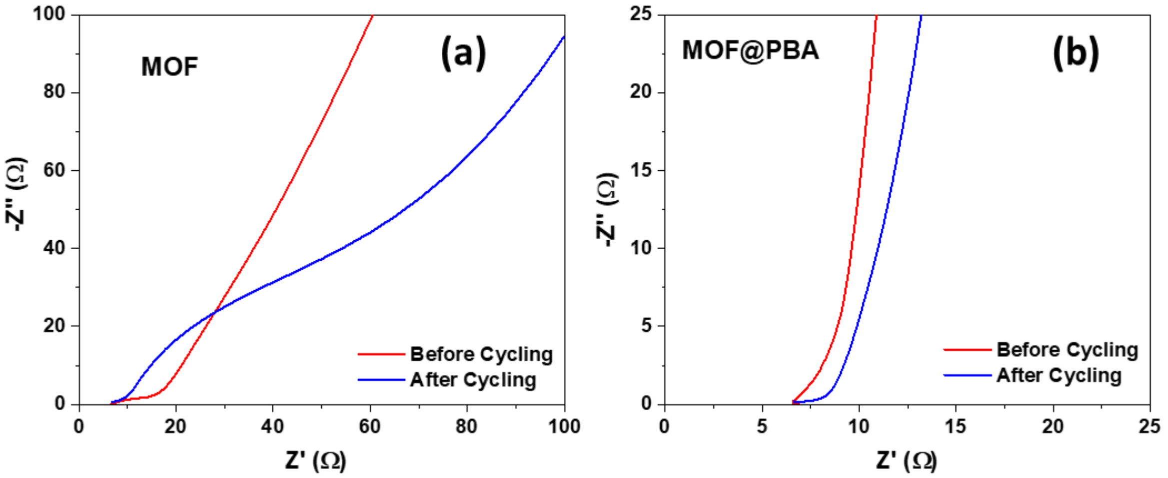

Figure S29: Nyquist plots at before and after cycling: (a) NCBMOF-12 and (b) NCBMOF@PBA-12.

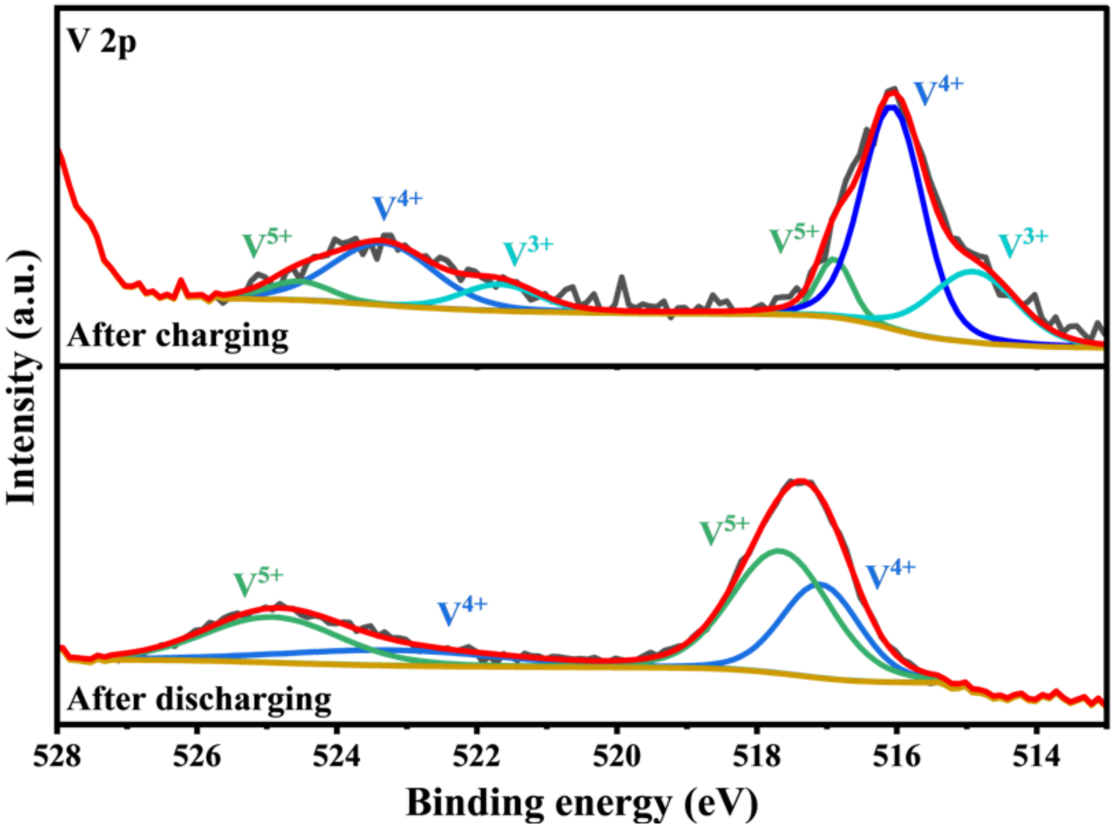

Figure S30: *ex situ* XPS analysis of AlVO@C at charged and discharged states, highlighting the V 2p spectra and corresponding changes in vanadium oxidation states during electrochemical cycling.

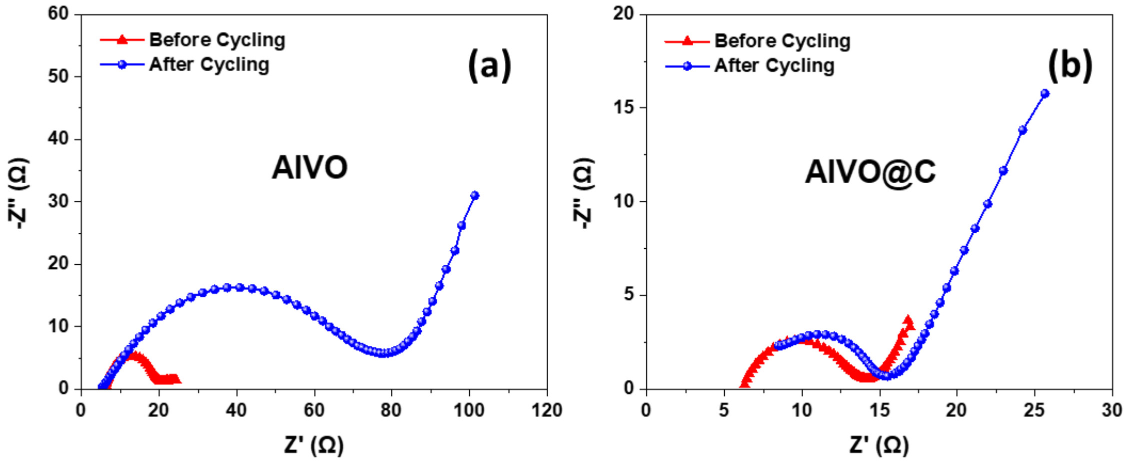

Figure S31: Nyquist plots at before and after cycling: (a) AlVO and (b) AlVO@C.

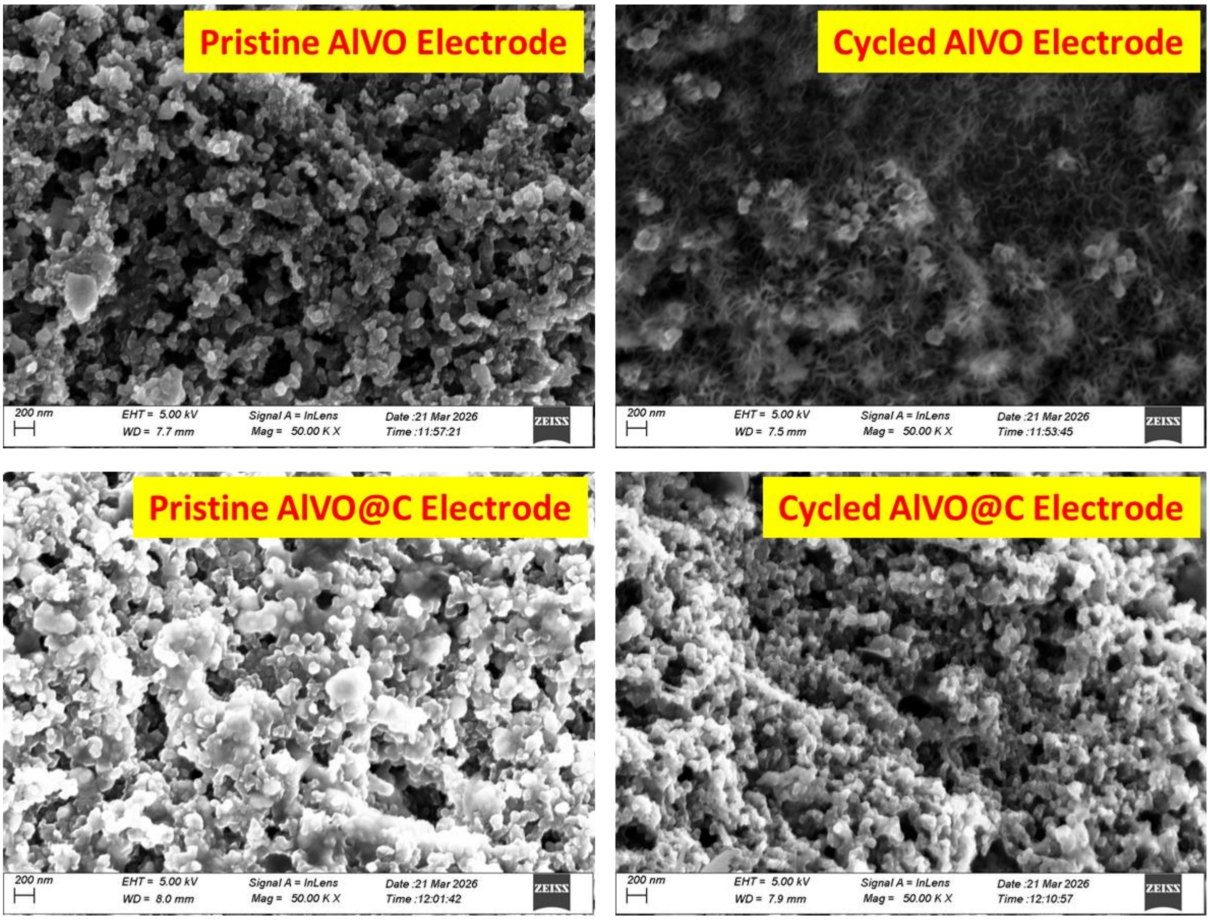

Figure S32: SEM images comparing the surface morphologies of AlVO and AlVO@C negative electrodes in their initial pristine state and after prolonged electrochemical cycling (50,000 CV at a scan rate of 25 mV s^{-1}). The AlVO electrode exhibits significant morphological degradation after CV cycling, including particle pulverization, surface roughening, and loss of structural integrity, which can be attributed to repeated volume expansion and contraction during Zn^{2+} insertion/extraction. In contrast, the AlVO@C electrode largely preserves its original morphology, maintaining particle integrity and surface uniformity even after extended cycling. This clear difference highlights the critical role of the carbon shell in buffering volume changes, stabilizing the electrode structure, and suppressing mechanical degradation.

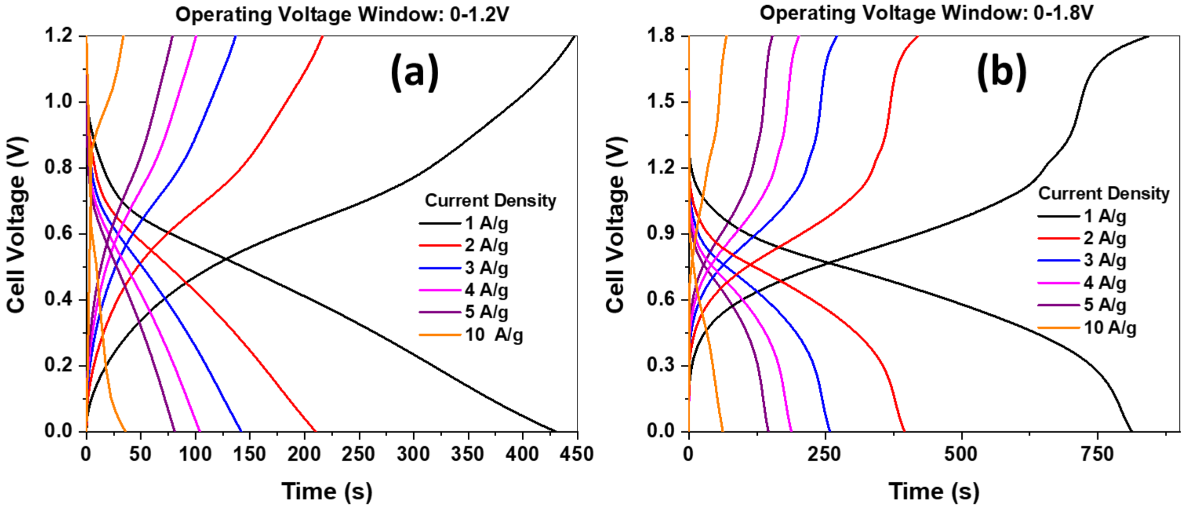

Figure S33: GCD profiles of the NCBMOF@PBA-12//AlVO@C full cells under (a) 0-1.2 V and (b) 0-1.8 V window.

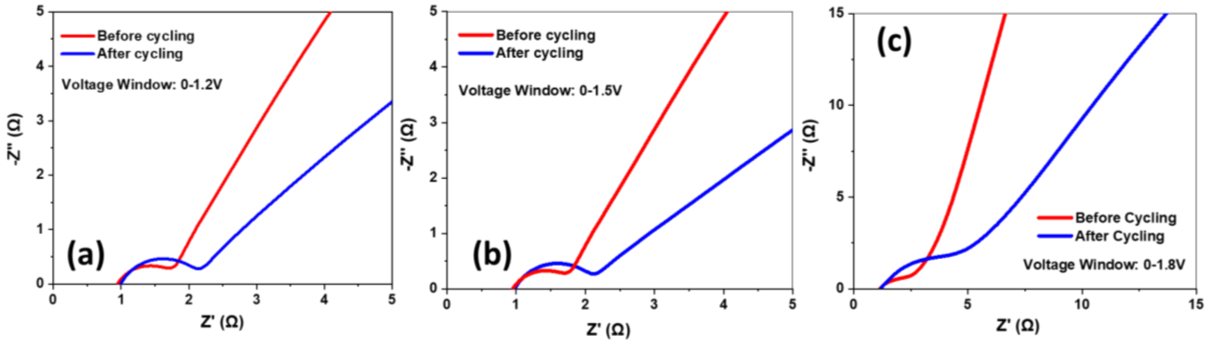

Figure S34: Nyquist plots at before and after full cell cycling at variable voltage regime: (a) 0-1.2 V, (b) 0-1.5 V, and (c) 0-1.8 V.

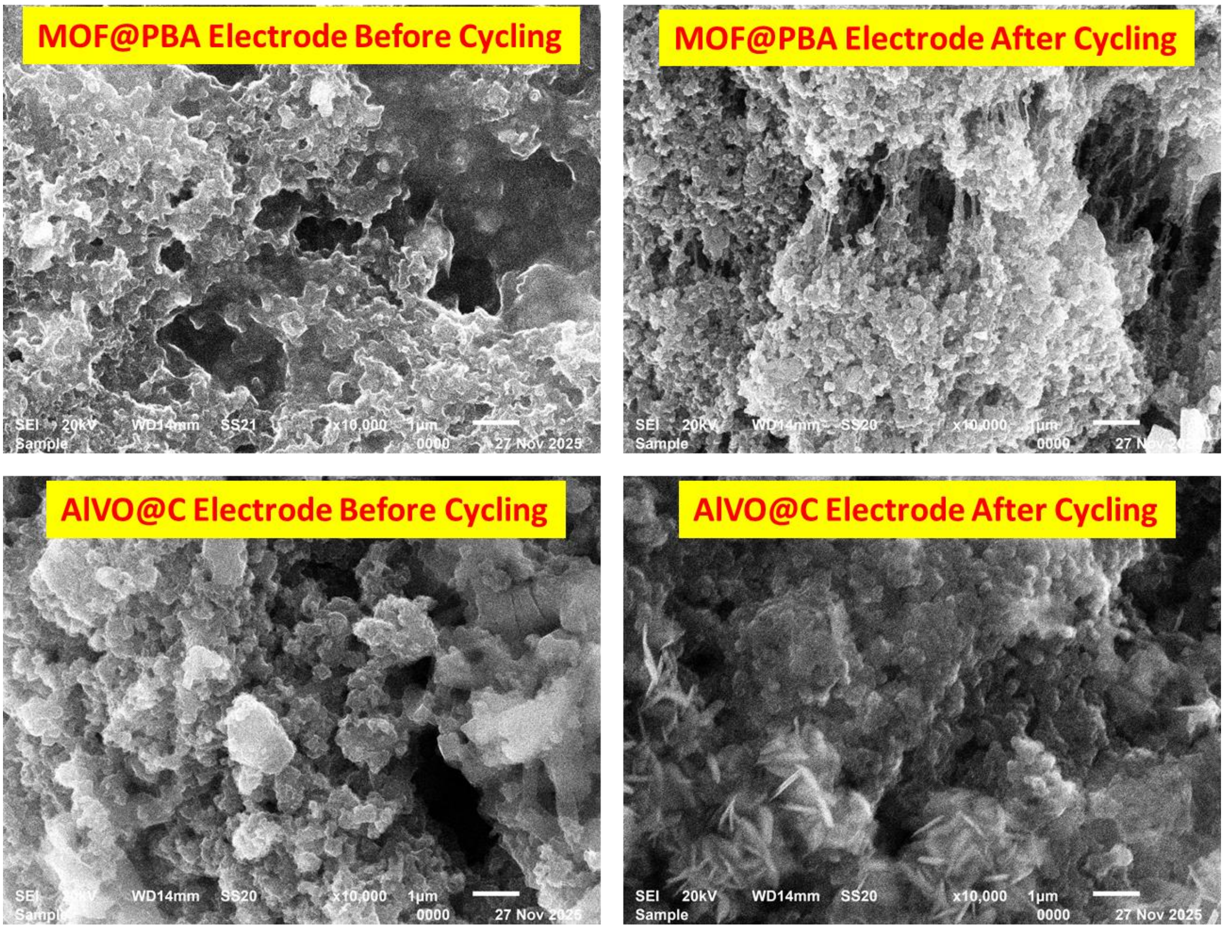

Figure S35: Surface morphology of NCBMOF@PBA-12 positive and AlVO@C negative electrodes at before and after cycling test @ 1 A g^{-1}. All images are in 10,000X magnification; and Scale bar = 1 μm.

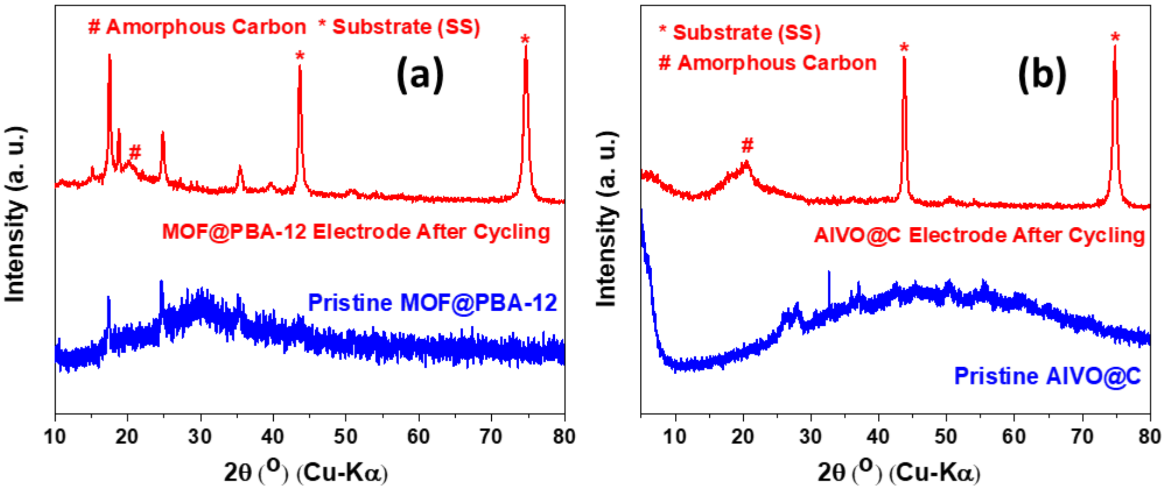

Figure S36: Comparative PXRD patterns of pristine active material and corresponding cycled electrodes (@ 1 A g^{-1}): (a) NCBMOF@PBA-12 and (b) AlVO@C, showing structural stability after cycling.

References

S1. P. Naskar, B. Biswas, S. Laha and A. Banerjee, *Energy Adv.,* 2024, **3**, 1401.

S2. P. Naskar, S. Mondal, B. Biswas, S. Laha and A. Banerjee, *J. Electrochem. Soc*., 2023, **170***, 090535*.

S3. K. Wang *et al*., *J. Alloy. Compd*., 2022, **901**, 163588.

S4. H. Li *et al*. *Chem. Eng. J*., 2022, **428**, 131071.

S5. Y. Shao *et al*. *Adv. Funct. Mater*., 2020, **31**, 2007843.

S6. F. Wei, H. F. Zhang, J. F. Wang, J. L. Zhuang and Y. H. Lv, *J. Alloy. Compd*., 2022, **907**, 164536.

S7. S. Wang *et al*. *Nanomicro Lett*., 2019, **11**, 70.

S8. Q. Yang *et al. ACS Nano,* 2019, **13**,8275–8283.

S9. Y. Jin *et al. Mater. Today Energy*, 2021, **19**, 100598.

S10. Z. Huang *et al*. *Angew. Chem. Int. Ed. Engl*., 2021, 60, 1011–1021.

S11. S. Zeng, X. Shi, D. Zheng, C. Yao, F. Wang,W. Xu and X. Lu, *Mater. Res. Bull.*, 2021, **135**, 111134.

S12. H. Zhang, Z. Chen, Y. Zhang, Z. Ma, Y. Zhang, L. Bai and L. Sun, *J. Mater. Chem. A*, 2021, **9**, 16565

S13. C. Leng, Z. Zhao, J. Guo, R. Li, X. Wang, J. Xiao, Y. V. Fedoseeva, L. G. Bulusheva and J. Qiu, *Chem. Commun.*, 2021, **57**, 8778.

S14. F. Ji, S. Gou, J. Tang, Y. Xu, S. M. Eldin, W. Mai, J. Li and B. T. Liu, *Chem. Eng. J.*, 2023, **474**, No. 145786.

S15. H. Ren, L. Zhang, J. Zhang, T. Miao, R. Yuan, W. Chen, Z. Wang, J. Yang and B. Zhao, *Carbon*, 2022, **198**, 46-56.

S16. Y. Wang, J. Cao, J. Guo , J. Zhang , G. Liu , D. Wang , W. Si , J. Song , X. Meng and G. Wen, *J. Alloys Compd.*, 2022, **915**, 165418.

S17. Z. Zou, H.Chen, Q. Li, Y. Wei, X.Zhang, X. Zou, X. Mei and J. Tao, *ACS Appl. Nano Mater.* 2024, **7**, 20645–20652.